Nonlinearity exponents in lightly doped conducting polymers

D. Talukdar,[1] U. N. Nandi,[2] K. K. Bardhan,[1,*] C. C. Bof Bufon,[3] T. Heinzel,[3] A. De,[1] and C. D. Mukherjee[1]

[1]*Saha Institute of Nuclear Physics, I/AF Bidhannagar, Kolkata 700 064, India*

[2]*Department of Physics, Scottish Church College, 1 & 3 Urquhart Square, Kolkata 700 006, India*

[3]*Heinrich-Heine-Universität, Universitätstrasse 1, D-40225 Dusseldorf, Germany*

(Received 22 March 2011; revised manuscript received 19 May 2011; published 11 August 2011)

The *I-V* characteristics of four conducting polymer systems such as doped polypyrrole, poly(3,4-ethylenedioxythiophene), polydiacetylene, and polyaniline in as many physical forms have been investigated at different temperatures, quenched disorder, and magnetic fields. Transport data clearly show the existence of a *single* electric-field scale in each system. Based upon this observation, a phenomenological scaling analysis is performed, leading to the extraction of a numerical value for a nonlinearity exponent called x_M which serves to characterize a set of *I-V* curves. The conductivity starts deviating from an Ohmic value σ_0 above an onset electric field F_o which scales according to $F_o \sim \sigma_0^{x_M}$. The electric-field-dependent data are shown to be described by the multistep tunneling model of Glazman-Matveev [JETP **67**, 1276 (1988)] in a near-perfect manner over nine orders of magnitude in conductivity and five orders of magnitude in electric field. Furthermore, x_M is found to possess both positive and negative values lying between $-1/2$ and $3/4$. There is no theory at present for this exponent. Some issues concerning applicability of the Glatzman-Matveev model are discussed.

DOI: 10.1103/PhysRevB.84.054205 PACS number(s): 72.20.Ht, 72.80.Le, 05.70.Jk

I. INTRODUCTION

Conducting polymers (CPs) such as doped polyacetylene (PA), polypyrrole (PPy), poly(3,4-ethylenedioxythiophene) (PEDOT), and polyaniline (PANI) show a great variety of transport properties. In general, the electronic structure of π-conjugated pristine (undoped) CPs originates from the sp^2p_z-hybridized wave functions of the carbon atoms in the repeat unit. Despite strong electron-phonon coupling in pristine CPs, an extraordinarily large range of conductivities has been covered by doping. Conductivity σ ranges from the highly insulating values 10^{-6} S/cm to highly metallic ones 10^5 S/cm depending on the doping concentration.[1] Such a wide range of conductivities has made CPs useful in many applications such as wires, electromagnetic interference shields, antistatic coatings, conducting layers in active devices including organic- and polymer-based light-emitting devices, photovoltaic devices, and field-effect transistors.[2–4]

The electronic transport properties of CPs are furthermore strongly influenced by the synthesis procedure and intrinsic disorder.[5,6] The conductivity of CPs originates from mobile charge carriers into the π-conjugated electronic orbitals which get filled by doping. At low doping densities, these charges self-localize to form solitons, polarons, and bipolarons.[7] At higher doping levels, a transition to a metallic state is typically observed.[8] Quite often, disorder dominates the macroscopic properties, thereby hiding or even eliminating the intrinsic delocalization along the chains.[9] However, no matter how well the chains are ordered, the electrons finally have to hop between chains, and the related local resistances strongly influence or even dominate the macroscopic conduction. This leads to an increase in conductivity as the temperature is increased, that is, an insulating behavior. Metallic behavior is observed only at larger temperatures and only in some polymer systems.[10] Thermoelectric power (TEP) measurements as a function of temperature, as well as anomalous differences between optical and dc conductivity data, provide evidence[11] that CPs can be treated as being structurally heterogeneous, consisting of thin, metal-like fibrils, separated by amorphous regions of width $\sim$5 nm.[12,13] This structural disorder is responsible for low electrical conductivities owing to low mobilities for most CPs, even though in fully doped polymers, charge carrier concentrations can be as large as $10^{23}/\text{cm}^3$, which is about four orders of magnitude higher than in highly doped inorganic semiconductors.

Polypyrrole has been particularly extensively investigated due to its many prospects for applications, such as relatively high environmental stability, high conductivity, or the simplicity of preparation either by chemical or by electrochemical polymerization.[14,15] Polypyrrole is an amorphous conjugated polymer based on an aromatic ring and has a nondegenerate ground state.[16] The polymer chains are intertwined and the fibrils are randomly oriented. Consequently, PPy systems must be regarded as three-dimensional disordered systems with respect to their structure and morphology. Over the last few years, PEDOT has attracted a lot of interest because of high conductivity, optical transparency, easy processability, and high stability.[17] Inganas and co-workers[18] have shown that PEDOT has a band gap of approximately 1.6 eV and can be cycled between the reduced and the oxidized state. It has been suggested that PEDOT has a lamellar-type structure built from ellipsoidal, conductive particles.[19] Even in highly conducting samples, one observes a mixture of insulating and metallic transport behavior. This has been explained in terms of a heterogeneous morphology.[11]

CPs are known to undergo a metal-insulator transition as a function of doping.[20] Samples at the insulating side of the transition are of interest here. Conduction data[21–25] in CPs at low fields in this regime are usually discussed within the framework of the standard Mott variable-range hopping (M-VRH) model[26] and its modification (ES-VRH) by Efros and Shklovskii[27] in presence of Coulomb interactions at low temperatures. The conductivity in any VRH model is given by

$$\sigma(T) = \sigma_m \exp\left[-\left(\frac{T_0}{T}\right)^m\right]. \quad (1)$$

Here σ_m is the conductivity prefactor and T the temperature. In the M-VRH model, the exponent m is given by $m = 1/(d+1)$, where d is the dimensionality. Thus, m is $1/4$, $1/3$, and $1/2$ in three, two, and one dimension, respectively. The characteristic temperature T_o is given by $T_o = 4\pi/3N(E_F)k_Ba^3$, where $N(E_F)$ is the density of states at the Fermi level, k_B the Boltzman constant, and a the localization length. In the ES-VRH model, interactions among electrons were shown to open up a Coulomb gap in the density of states at the Fermi level. This leads to $m = 1/2$ independent of the dimension and

$$T_o = \frac{2.8e^2}{4\pi\epsilon_0\epsilon k_B a}, \tag{2}$$

where ϵ is the dielectric constant. The standard VRH model seems to describe well three-dimensional systems such as powdered $FeCl_3$-doped PPy[21] and PEDOT at higher temperature,[22] yielding $m = 1/4$. PTS-doped PPy films[23] are reported to yield $m = 1/3$, suggesting a two-dimensional nature. The exponent in single crystals of PTS-doped polydiacetylene (PDA)[24] is found to be ~0.65–0.70, apparently demonstrating the quasi-one-dimensional nature of the system. On the other hand, some samples such as PEDOT at low temperature[22] and PPy films[25] tend to follow ES-VRH, particularly at low temperature with $m = 1/2$.

Non-Ohmic or nonlinear conduction is a very common feature of disordered systems in general and CPs in particular. Onset of nonlinearity in these systems often takes place upon application of only few volts of bias across samples in laboratories. In bulk systems, this is rendered possible by the presence of microscopic inhomogeneties, which lead to very large local fields. Now, with the advent of low-dimensional materials such as nanotubes, nanofibers, nanowires, and quantum dots, the generation of large fields with moderate bias applied across small lengths are quite common. This provides added incentive to study and understand the phenomena of nonlinear conduction in CPs. Nonlinear transport data in CPs[15,24,25,28–33] are either presented in the form of I-V curves or, equivalently, in the form of Σ-V curves, measured as a function of temperature. However, there are hardly any systematic analyses of the data, mainly because theoretical understanding[28,34–39] is far from complete. For example, the models of variable range hopping under field[34–37] have expressions for the field-dependent conductivity in two field limits—low or moderate and high—as a function of temperature. Glazman and Matveev (GM)[39] have evaluated a model involving multistep tunneling across thin disordered regions in two limits, $eV \gg k_BT$ and $eV \ll k_BT$. In the first limit, one has at any temperature a full expression for $\Sigma(V)$ containing parameters without having any temperature dependence. In rest of the paper, we use the symbol σ for conductivity and Σ for conductance which here is taken as the chordal conductance, I/V, unless otherwise mentioned.

In this paper, we present electrical transport measurements covering both linear and nonlinear regimes in moderately doped PPy in forms of pellets as well as films and in a pellet of doped PEDOT over a wide range of temperatures. In addition, some published data from literature have been also processed for comparison. For analysis of our data, we depart from methods used in existing literatures and adopt a newly suggested methodology[40] based upon observation of existence of a field scale in many disordered samples. This method of scaling analysis of a set of I-V curves yields an exponent x_T, called nonlinearity exponent, that characterizes the nonlinear data and is believed to reflect the underlying field-dependent conduction mechanism. We apply this scaling approach to various CP systems, examine its validity, and extract the nonlinearity exponents. In the next section (Sec. II), the method of scaling analysis is described in detail. Furthermore, various results of VRH under field are also reviewed along with corresponding experimental results reported in the literature. The GM model[39] was originally developed for mesoscopic thin amorphous films whose dimensions along the hopping direction (i.e., thickness) lie between the localization lengths and hopping lengths and is applied here to explain nonlinear data in CPs. These models are critically discussed in particular context of the general requirements of scaling. Since the GM expression is found rather surprisingly to be very successful in explaining the I-V characteristics in CPs, this section includes details of phenomenological adaption leading to the scaling version of the model for macroscopic samples. Experimental details are given in Sec. III. Data are presented and analyzed mainly by adapting the GM expression as a scaling function in Sec. IV. Results so obtained are then discussed in Sec. V, which also contains a subsection taking a critical look at the applicability of GM model to macroscopic systems such as considered in this work. Finally, conclusions are given in Sec. VI.

II. SURVEY OF MODELS OF NONLINEAR CONDUCTION: THEORETICAL AND PHENOMENOLOGICAL

A study of field-dependent conduction is generally expected to bring out subtleties or additional processes that are either not present or insignificant in the linear conduction. Consider, for example, composites which are random mixtures of conductors and insulators above the percolation threshold. For small bias, conduction takes place only through the backbone and is Ohmic. As the bias is increased, tunneling across the thin insulating layer between the ends of the conductor chains dangling off the backbone are believed to lead to increased conductance.[41] In view of the inadequate theoretical development, it should be of much utility to know general properties of nonlinear conduction. One can then check whether any specific theoretical model prediction is consistent with general requirements or not. One general property is that the conductance $\Sigma(F)$ always increases with field F, at least at small fields. This property is obvious since the application of a field results in lowering barrier heights, thus decreasing resistance to conduction. For a proper description, one defines a characteristic field or a field scale F_o such that $\Sigma(F) \geqslant \Sigma(0)$ for $F \geqslant F_o$. This corresponds to the fact that a sample remains Ohmic at small fields and starts deviating from the Ohmic behavior as the field is increased beyond F_o. The scale may be also formally given by the following $[\Delta\sigma(F) = \sigma(F) - \sigma(0)]$:

$$\Delta\sigma(F_o) \sim \sigma(0). \tag{3}$$

I-V curves are generally measured as a function of some physical parameter upon which $\sigma(0)$ depends. Temperature is the most commonly used parameter. Others such as magnetic field and pressure are also valid parameters. An interesting but less studied situation is when I-V data are gathered simply as

a function of quenched disorder as in composite samples.[41] Naturally, F_o is expected to be a function of the parameter.

A. Scaling analysis: Nonlinearity exponent

Let us consider, for definiteness, cases where measurements are carried out at different temperatures. Recently, a generalized approach[40] based on existence of a *single* field scale in a given disordered sample has been adopted, leading to characterizing a set of *I-V* curves by a number x_T, called nonlinearity exponent. In this approach, the conductivity $\sigma(T,F)$ is given by the one-parameter scaling relation:[40]

$$\frac{\sigma(T,F)}{\sigma(T,0)} = \Phi\left(\frac{F}{F_o}\right), \tag{4}$$

where Φ is a scaling function. The field scale $F_o(T)$ is assumed to vary with the linear conductivity as

$$F_o(T) = A_T\ \sigma_o(T)^{x_T}, \tag{5}$$

where $\sigma_o(T) = \sigma(T,0)$ is the linear conductivity at temperature T and A_T is a constant whose value depends upon how the scale F_o is chosen. At small fields, $q = F/F_o \leqslant 1$, the scaling function $\Phi(q) \approx 1$ corresponding to the fact that the conductance increases very little from the zero field value σ_o. At larger fields $q > 1$, $\Phi(q) > 1$. Thus, the field F_o can be called a crossover or onset field such that it separates the linear regime from the nonlinear regime along the field axis. Whereas the choice of temperature-dependent linear conductivity as the relevant variable in Eq. (5) is similar to the one in the scaling theory of localization,[42] the power law is standard in the theory of critical phenomena.[43] Note that temperature does not enter *explicitly* in Eq. (5) but does so through the temperature-dependent $\sigma_o(T)$. Thus, according to Eq. (5) the field scale for nonlinearity is determined solely by the linear conductivity σ_o. This is quite significant in that the same relation holds good even when σ_o is changed by some other variable such as magnetic field or simply quenched disorder [see Eq. (7)]. Presently, a theoretical foundation of this result is lacking but diverse disordered systems with localized states[40] including amorphous and doped semiconductors, composites at low temperatures have been found to obey such scaling.

Equation (5) leads to a power-law variation of conductivity at large fields $F \gg F_o$, where *I-V* curves often tend to become independent of temperature or rather σ_o. It is seen from Eq. (4) that the latter is readily ensured if $\Phi(q) \sim q^{1/x_T}$ at large q for $x_T > 0$. Thus, at large fields the conductivity varies as a power law with an exponent z_T:

$$\sigma(T,F) \sim F^{z_T}, \quad z_T = 1/x_T \quad \text{for} \quad x_T > 0. \tag{6}$$

This prediction provides a self-consistency check for the positive exponent x_T as it may be determined using two independent methods: one from a set of *I-V* curves at low fields and the other from a single *I-V* curve at high fields. This has been also amply verified[40] in systems mentioned earlier. It is also clear that in case of negative x_T one cannot expect temperature-independence of conductivity at large field.

Composite systems at room temperature are presently the only disordered ones where the nonlinearity exponent has been explained,[44,45] although they are not, strictly speaking, comparable to the systems under study in this paper. Nevertheless, it may be instructive to review non-Ohmic conduction in these systems. In this case, *I-V* curves have been measured at a *fixed* temperature (i.e., room temperature) in samples with various degree of disorder characterized by the parameter p, fraction of conductors in a sample. Just above the percolation threshold p_c (i.e., $p \geqslant p_c$), *I-V*'s turn out to be nonlinear even at room temperature with conductance increasing with the applied bias. As mentioned earlier, the increase in conductance is due to opening up of new channels of conductions, from tunneling across closely spaced tips of pairs of branches of conductors dangling off the backbone. The bias scale[44] was found to vary as the inverse of the correlation length ξ,

$$V_o(p) \leqslant \xi^{-1} \sim {\Sigma_o}^{\nu/t}, \tag{7}$$

so that the nonlinearity exponent x_p is given by $x_p \leqslant \nu/t$ where ν and t are the correlation and conductivity exponents, respectively, and $\Sigma_o(p) = \Sigma(p, V = 0) \sim (p - p_c)^t$. The subscript in the exponent denotes the parameter that is varied to change Σ_o. ν/t is about 0.45 in three dimensions and consistent with the values of x_p obtained experimentally in discontinuous gold film[44] and carbon wax.[45]

It is seen from Eqs. (5) and (6) that the nonlinearity in a system can be characterized by two quantities: the field scale F_o that determines the onset and the nonlinearity exponent x_M that determines the degree (i.e., steepness of increase of the conductivity with field). Here M stands for the variable(s) used to vary $\sigma_o(M) = \sigma(M, F = 0)$. Both the scaling function Φ and the nonlinearity exponent x_T are obviously determined by the details of the conduction mechanism under study. Let us now consider some models and see how they conform to general scaling formulation.

B. Variable range hopping under field

In disordered systems, an increasing electric field aligns an increasing number of empty and accessible states to the occupied states, allowing charge carriers to move via phonon-assisted tunneling or hopping transitions. With decreasing temperature the mean hopping length R_h grows as

$$R_h = \frac{a}{2}(T_o/T)^m, \tag{8}$$

where T_0 and m are the same as in Eq. (1). With higher electric fields the energy eFR_h gained by an electron may become comparable to k_BT and lead to deviation from Ohmic behavior. Theories[34,36,37] predict two characteristic fields F_l and F_u such that the non-Ohmic conductivity at intermediate fields $F < k_BT/ea$ is given by

$$\sigma(T,F) = \sigma(T,0)\ \exp\left(\frac{eFL}{k_BT}\right), \tag{9}$$

where $\sigma(T,0)$ is given by Eq. (1) and L is a length related to the hopping length R_h. Clearly, $F_l = k_BT/eL$ could be identified with the onset field scale F_o discussed above. L is proportional to R_h^μ, where μ is either 1 (Refs. 34 and 36) or 2 (Ref. 37). Thus, it follows from Eqs. (9) and (8) that F_o varies with T as a power law,

$$F_o \approx F_l \sim T^\alpha/a{T_o}^{\alpha-1}, \quad \alpha = 1 + m\mu, \tag{10}$$

with the same m as in Eq. (1). According to Eq. (10), the exponent α is always positive and greater than 1. In the literature, however, authors traditionally focus on the temperature dependence of $L \sim T^{-m\mu}$ rather than the field scale. The compliance of this with experimental results[46] in amorphous and doped semiconductors is rather poor. In many cases the power law (i.e., a straight line in a log-log plot of F_o vs T) is not observed. When the plot appears like a straight line, the exponent often turns out to be randomly different from the expected value in Eq. (10), albeit with few exceptions. In the limit of large fields $F \geqslant k_B T/ea$ theories[35,36] agree with "activationless" hopping, at least qualitatively. In such situation the conductivity becomes independent of temperature and is given by

$$\sigma \sim \exp\left[-\left(\frac{F_u}{F}\right)^m\right], \quad F_u = a_1 \frac{k_B T_o}{ea}, \tag{11}$$

with the same m and T_o as in Eq. (1). a_1 is a numerical constant equal to unity[35] when $m = 1/4$. Activationless hopping has been observed by many authors[46] irrespective of the value of m. However, inexplicably, the particular expression of high field conductivity in Eq. (11) has been found so far *only* in systems with $m = 1/2$. On the contrary, in several systems[47] with $m = 1/4$, the field dependence is well described, albeit empirically, by a power law $\sigma \sim F^z$ reminiscent of Eq. (6). As mentioned earlier, Eqs. (11) and (2) illustrate the possibility of having self-consistent relations involving the same parameters such as a, and T_o. This has led to quantitative disagreement[25,48] in that experimental values of F_u turn out to be always greater than the calculated ones. More significantly, it is to be noted that the large field conductivity as given by Eq. (11) is not compatible with the scaling Eq. (4).

C. Multistep tunneling

Considering the process of multistep indirect tunneling via n-localized states in a disordered system, GM proposed the following expression[39] for the conductance through an amorphous semiconductor thin film (i.e., tunnel barrier) of thickness w under bias V [$eV \gg k_B T$ and $p_n = n - 2/(n+1)$]:

$$\begin{aligned}\Sigma &= \Sigma_d + \Sigma_1 + \sum_2^n \Sigma_n V^{p_n} \\ &= \Sigma_0 + \Sigma_2 V^{4/3} + \Sigma_3 V^{5/2} + \Sigma_4 V^{18/5} \\ &\quad + \Sigma_5 V^{14/3} + \Sigma_6 V^{40/7} + \cdots,\end{aligned} \tag{12}$$

where $\Sigma_0 = \Sigma_d + \Sigma_1$. Σ_d accounts for the direct tunneling and Σ_1 for the elastic resonant tunneling via one localized state. Each term ($n \geqslant 2$) in the series arises out of rare events when a number of localized states happen to be arranged physically as well as energetically in such a way that an electron can traverse a sample length via multistep inelastic tunneling. Each term may be thought to constitute a separate channel of conduction involving a definite number of localized states. Thus, the macroscopic nonlinearity in this GM model results from two contributions: primarily, appearance of a new channel with increasing bias and, secondarily, nonlinearity of each such channel. This multistep tunneling model has been widely invoked to explain relevant data in various tunnel junctions[49,50] and manganites.[51,52] Interestingly, the manganites samples were not necessarily in the form of junctions. Nevertheless, it was thought fit to apply the GM model because of possibilities of tunneling across grain boundaries, or insulating barriers, separating metallic phases within samples. Considering the similar structure of CPs, that is, the polymer fibrils consisting of quasimetallic lengths with intervening insulating regions,[12,13] CPs are expected to be also candidates for application of the GM model. It is shown below how a couple of assumptions about the coefficients Σ_n make the GM expression Eq. (12) not only compatible with the general scaling formulation Eq. (5) but also yield the same relation between the nonlinearity exponent x_T and the large field exponent z_T as in Eq. (6).

1. Scaling

While the I-V data[49,51,52] at different temperatures have been fitted well by Eq. (12) with few nonlinear terms, no attempt was made to analyze systematically the temperature variation of the coefficients Σ_n ($n \geqslant 2$). In fact, in the limit $eV \gg k_B T$ in which Eq. (12) is valid, the coefficients are supposed to be independent of temperature but functions of thickness w and other parameters such as localization length a, etc., related to disorder. The contribution of the nth channel to the conductance is given by[39]

$$\Sigma_n V^{p_n} \propto C_n \left(\frac{V}{V_1}\right)^{n-1} \left(\frac{V}{V_2}\right)^{\frac{n-1}{n+1}} \exp\left[-\frac{2w}{a(n+1)}\right], \tag{13}$$

where $C_n \approx (n-1)^{n-1}$, ${V_1}^{-1} = ga^2we$, g is the density of localized states near the Fermi level, e is the electronic charge, ${V_2}^{-1} = \lambda_{ep} e/W_b$, λ_{ep} is a dimensional quantity dependent on electron-phonon coupling and other material constants, and W_b is the depth of the localized states. It is clear from the above equation that the GM expression Eq. (12) derived under various assumptions does not possess a channel-independent voltage scale as $V_1 \neq V_2$. Nevertheless, to make contact with experiments in macroscopic samples (see Sec. IV), we postulate that

$$\Sigma_n = c_n \, \Sigma_o {V_o}^{-p_n}, \tag{14}$$

for $n \geqslant 2$. Equation (14), when put in Eq. (12), makes the latter immediately compatible with the scaling Eq. (4):

$$\begin{aligned}\frac{\Sigma}{\Sigma_o} &= 1 + c_2\left(\frac{V}{V_o}\right)^{4/3} + c_3\left(\frac{V}{V_o}\right)^{5/2} + c_4\left(\frac{V}{V_o}\right)^{18/5} \\ &\quad + c_5\left(\frac{V}{V_o}\right)^{14/3} + c_6\left(\frac{V}{V_o}\right)^{40/7} + \cdots.\end{aligned} \tag{15}$$

The above expression explicitly implies the existence of a single bias scale V_o as in Eq. (4) provided that c_n's are constants independent of Σ_o. c_n's are, by definition, always positive quantities. The right-hand side of the above equation is thus really a scaling function Φ as defined in Eq. (4). The same should hold if conductivity and field are used in place of conductance and bias provided that the sample sizes are large enough to ensure length-independent conductivities. It is seen from Eq. (14) that the constants c_n are determined once the coefficients Σ_n and the scale V_o are known. The expression Eq. (15) suggests that experimental Σ-V curves at different

T's may be collapsed into a single curve by suitable choices of Σ_o and bias scale V_o at each temperature. Note that at $V = V_o$, the coefficients c_n's satisfy the following relation:

$$\frac{\Sigma(V_o)}{\Sigma_o} = 1 + \sum_2^n c_n. \tag{16}$$

If, for example, $\Sigma(V_o) = 2\Sigma_o$, we have $\sum_2^n c_n = 1$.

2. *Nonlinearity exponent x_T*

The voltage scale V_o can be defined in a more intuitive way in the following manner. Let $n = n_o$ be the lowest channel with nonzero Σ_{n_o}. From Eqs. (3) and (12), V_o is given by $\Sigma_{n_o} {V_o}^{p_{n_o}} \sim \Sigma_o$, which leads to the expression for V_o as

$$V_o \sim \left(\frac{\Sigma_o}{\Sigma_{n_o}}\right)^{1/p_{n_o}}. \tag{17}$$

This is consistent with the more general assumption Eq. (14). At this point, we make the second postulate that Σ_n follows a power-law behavior with Σ_0 as given by

$$\Sigma_n \sim {\Sigma_o}^{y_n}, \tag{18}$$

where y_n is an exponent. Interestingly, in the GM model if the contribution from direct tunneling to the Ohmic conductance, $\Sigma_d \sim \exp(-2w/a)$, can be neglected compared to that from resonant tunneling, $\Sigma_o \sim \exp(-w/a)$ as in case of thick barrier $(w/a \gg 1)$, then we have $\Sigma_o = \Sigma_d + \Sigma_1 \approx \Sigma_1 \sim \exp(-w/a)$. Neglecting other slow varying functions of n in Eq. (13) yields Eq. (18), with

$$y_n = \frac{2}{n+1}, \tag{19}$$

for $n \geqslant 2$. Thus, y_n is always less than 1, being 0.67 for $n = 2$, 0.5 for $n = 3$, and so on in mesoscopic systems. As seen later, these values of y_n are incompatible with the results in macroscopic samples. Incorporating Eq. (18) in Eq. (17) and comparing with Eq. (5), one has

$$x_T = \frac{1 - y_{n_o}}{p_{n_o}} = \frac{1 - y_n}{p_n} \tag{20}$$

for any $n \geqslant 2$. The second equality on the right-hand side of the above equation follows from Eqs. (14) and (18). Notice that while the left-hand side of Eq. (20) is a constant, the right-hand side carries the index n. Thus, if $n_o = 2$, then $x_T = \frac{3}{4}(1 - y_2)$. If $n_o = 3$, then $x_T = \frac{2}{5}(1 - y_3)$, and so on. Incidentally, putting Eq. (19) into Eq. (20) yields $x_M = 1/(n+2)$, a channel-dependent quantity instead of a constant value. All three phenomenological relations, Eqs. (5), (14), and (18), only two of which are independent, underline a basic assumption that nonlinear scales are determined by the corresponding linear conductivity. Equation (20) is remarkable for several conclusions that immediately follow from it.

(i) x_T is 0 when $y_{n_o} = 1$. It is positive or negative depending upon whether y_{n_o} is less than or greater than 1. Furthermore, its maximum possible value is $1/p_2$ or 0.75 since the lowest value of p_n is 4/3 for $n = 2$. The lower limit of $-1/2$ is obtained from general arguments.[40] Thus, we have $-1/2 \leqslant x_T \leqslant 3/4$.

(ii) Since the left-hand side of Eq. (20) is independent of n, and p_n increases with n, it follows that for $x_T > 0$, y_n must decrease with n and for $x_T < 0$, y_n must increase with n:

$$\begin{aligned} 1 \geqslant y_2 \geqslant y_3 \geqslant \cdots \geqslant y_n, \quad x_T \geqslant 0, \\ 1 < y_2 < y_3 < \cdots < y_n, \quad x_T < 0. \end{aligned} \tag{21}$$

Thus, for $x_T < 0$, we have $x_T = -y_n/p_n$ for $y_n \gg 1$ at large n. If any Σ_n in the GM expression is zero, the corresponding y_n is obviously excluded from the above. It may be noted that y_n's given by Eq. (19) do satisfy the inequalities above for positive x_T.

(iii) For $x_T > 0$, the above naturally raises question about the limit of y_n for large n. Considering the fact that the conductance of a hopping system at large bias may tend to become independent of T or, in other words, Σ_0, the lower limit of y_n may be taken as zero; that is, as $n \to \infty$, $y_n \to 0$. The limit is in agreement with Eq. (19). Note that y_n is always a positive quantity since the coefficient Σ_n is predicted to be a decreasing function of n.[39]

(iv) Since p_n increases with n, Eq. (20) requires that for $x_T > 0$, the series Eq. (12) must terminate at $n = n_L$, where the highest channel n_L is given by $p_{n_L - 1} < 1/x_T \leqslant p_{n_L}$.

3. *Large bias exponent z_T*

If the field-dependent conductance of a system continues to be described by Eq. (12) (e.g., there is no appearance of negative differential conductance), it follows that at large bias or field the conductance varies with bias as a power law: $\Sigma \approx \Sigma_{n_L} V^{p_{n_L}}$, where n_L is the index of the highest allowed channel [see item (iv) above]. Such a power-law variation is also predicted by the scaling consideration Eq. (6) for $x_T > 0$ with $z_T = p_{n_L}$. Now, from Eq. (20), we obtain $x_T = (1 - y_{n_L})/p_{n_L}$ so that $z_T = (1 - y_{n_L})/x_T \cong 1/x_T$ following item (iii). Thus, we obtain $z_T \cong 1/x_T$ as follows from general scaling consideration [Eq. (6)]. Since $|x_T| < 1$, $z_T > 1$.

III. EXPERIMENTAL

The three systems used in this study were doped PPy in powder and film forms and doped PEDOT in powder form. All together five samples (see Table I) have been studied. All samples were synthesized using chemical polymerization. To aqueous solution of pyrrole monomer (0.05M), 100 ml of aqueous $FeCl_3$ (0.1M) solution was added dropwise leading to almost instant polymerization. Black precipitate of PPy was separated from the solution and the resulting powder was then vacuum dried and pressed into disk-shaped pellets, 8 mm in diameter and 1 mm in thickness (sample 1). Further details can be found in Ref. 21. A similar procedure was followed for synthesis of doped PEDOT (sample 2) using monomer ethylenedioxythiophene (EDOT) dissolved in water with 0.2M dodecylbenzenesulfonic acid. Subsequently, an aqueous solution of the oxidizing agent $FeCl_3$ was added dropwise on constant stirring under inert atmosphere. EDOT:$FeCl_3$ molar ratio was 1.167:1. After overnight reaction, the precipitate was thoroughly washed with ethanol, vacuum dried, and pelletized in form of disks of same dimensions as above. PPy films (samples 3–5) were synthesized from pyrrole vapor in solutions of HCl:H_2O_2 = 1:1000, while the solvent was cooled

TABLE I. Sample growth conditions and parameters Eq. (1).

System	Sample No.	Oxidant	σ_o (300 K) (S/cm)	m	T_o (K)
PPy (powder)	1	$FeCl_3$	5.7×10^{-4}	1/4	1.7×10^6
PEDOT (powder)	2	$FeCl_3$	2.6×10^{-2}	1/2	1798
PPy (film)	3	$HCl:H_2O_2$	10	1/2	2340
PPy (film)	4	$HCl:H_2O_2$	12	1/2	950
PPy (film)	5	$HCl:H_2O_2$	8.5	1/2	1600

to 282 K, 283 K, and 300 K, respectively. Further details can be found in Ref. 25 (sample 3 here is the same as sample A in the latter). Thicknesses were 70, 77, and 60 nm, respectively.

Table I shows typical room-temperature conductivities of the samples. For transport measurements, thin copper wires were attached to both ends of the disks using silver paint, whereas leads were connected to prepatterned Pt electrodes on the substrate containing PPy film.[25] Two- and four-probe dc transport measurements gave similar results, indicating negligible contact resistances in samples. Low-temperature measurements were done in liquid helium cryostats in the temperature range 2.1 K–300 K. The PPy and PEDOT samples were placed on sapphire substrates with Apeizon N-grease and data were taken under the constant current condition. In case of PPy films, data were taken under the constant voltage condition. Temperature was stabilized to better than ±50 mK for the *I-V* measurements. Maximum current levels were kept low to minimize joule heating in the samples. For example, the maximum current through the PEDOT sample at 26 K was limited to 0.22 mA as an increased current led to instability due to joule heating. However, this behavior was completely reversible and sample resistance returned to the initial value after removal of current.

IV. RESULTS

Figure 1 shows Ohmic conductivities σ_o vs T^{-m} for four samples: one each of PPy (powder) and PEDOT and two of PPy (film). Similar data for sample 3 have been already presented in Ref. 25. Excellent linearity in the data shows that all the samples obey variable range hopping conduction in the range of temperatures measured. While m is 1/4 in PPy (powder), it is 1/2 in all samples of other two systems. The different values of m in PPy samples may be due to different measurement ranges of temperature: 80 K–300 K for the powdered sample and 2.1 K–20 K in films. There is a transition at 30 K in PPy films from ES-VRH mechanism to activated process. A similar transition from ES-VRH to M-VRH also takes place in PEDOT at about 38 K. All the samples were in insulating regimes. T_0's obtained from slopes of the fitted lines are of the order of 10^3 K and are given in Table I. The exponent 1/2 has been shown to result from Coulomb gap at the Fermi level.[27] Parameters (i.e., m, T_o) in PPy (powder) and PEDOT agree with those reported earlier.[21,22] Values of selected $\sigma_o(T)$'s are given in Table II. It is seen from Table I that of the first three samples, the sample 1 (PPy powder) has the least conductivity at room temperature while the sample 3 (PPy film) has the highest. We discuss the systems in this order as the maximum normalized conductivity (see below) also follows the same order.

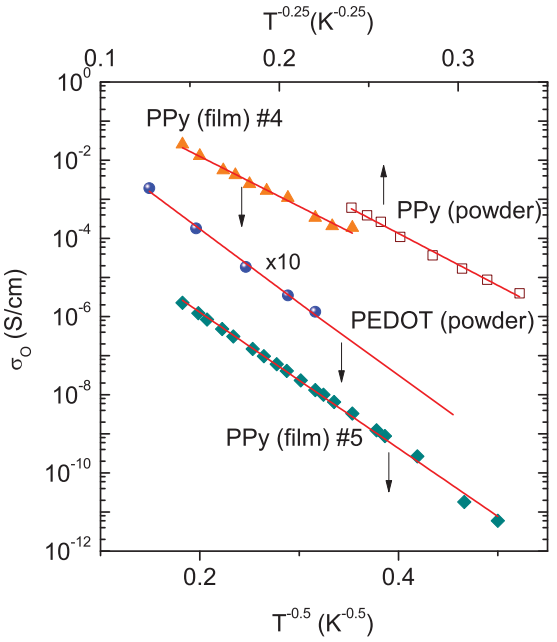

FIG. 1. (Color online) Variation of Ohmic conductivity σ_0 vs T^{-m} with $m = 1/4, 1/2$ for four CP samples as shown. For clarity, the PEDOT data have been shifted upward by a factor as shown. Solid lines are linear fits to the data.

A. Polypyrrole (powder)

The field dependence of dc conductivity σ of a PPy (powder) sample at different temperatures ranging from 80 K to 300 K are shown in Fig. 2. The nonlinear response of conductivity to the application of electric field can be clearly seen from the figure. The sample had a zero-bias linear conductance Σ_0 of 0.003 S at room temperature. A typical behavior at a constant temperature is that the conductivity

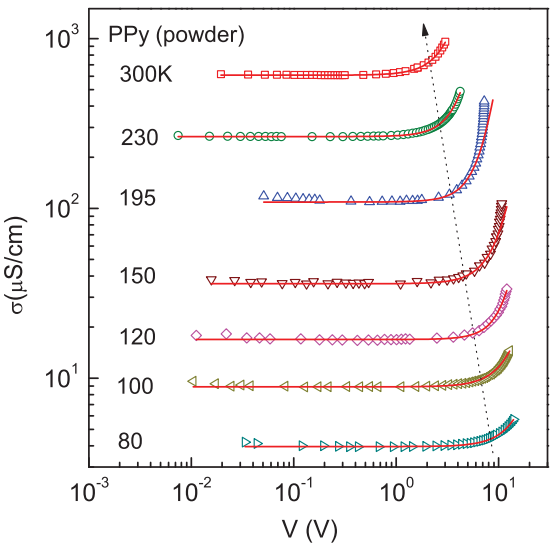

FIG. 2. (Color online) Variation of conductivity vs electric field in a doped PPy pellet (sample 1) at different temperatures, as indicated. The dotted line schematically indicates the movement of the onset bias with increasing temperature. The solid lines are fits to the GM expression Eq. (12). See text for details.

TABLE II. Parameters in GM expression Eq. (12) fitted to conductivity data at various temperature in five samples of three CP systems. σ_n ($n \geqslant 2$) is in unit of S/cm $V^{n-2/(n+1)}$. c_n's are constants defined by Eq. (14).

Sample	T (K)	σ_0 (S/cm)	σ_2	σ_3	σ_4	σ_5	σ_6	c_2	c_3	c_4	$c_5(c_6)$
PPy	80	3.96×10^{-6}		2.10×10^{-9}		1.30×10^{-12}			0.61		0.19
(powder)	100	8.96×10^{-6}		1.41×10^{-8}		6.50×10^{-12}			0.66		0.17
	120	1.69×10^{-5}		1.96×10^{-8}		8.62×10^{-11}			0.40		0.62
1	150	3.67×10^{-5}		1.16×10^{-7}		2.88×10^{-10}			0.58		0.34
	195	1.09×10^{-4}		6.90×10^{-7}		8.72×10^{-9}			0.44		0.49
	230	2.66×10^{-4}		3.23×10^{-6}		1.18×10^{-7}			0.48		0.42
	300	6.11×10^{-4}		1.63×10^{-5}		4.89×10^{-7}			0.58		0.25
PEDOT	4.9	5.30×10^{-10}	9.30×10^{-10}		3.06×10^{-11}			1.03		0.014	
(powder)	6.5	5.60×10^{-9}	6.11×10^{-9}		8.38×10^{-11}			1.06		0.014	
	10	1.33×10^{-7}	6.48×10^{-8}					0.94			
2	12	3.53×10^{-7}	1.38×10^{-7}					0.96			
	16.5	1.89×10^{-6}	5.23×10^{-7}		4.53×10^{-9}			0.94		0.065	
	26	1.80×10^{-5}	2.76×10^{-6}		7.57×10^{-7}			0.78		3.447	
PPy	2.1	8.00×10^{-16}	$\sim 8.8 \times 10^{-13}$		$\sim 8.0 \times 10^{-10}$		5.0×10^{-8}	~ 0.36		$\sim 3.7 \times 10^{-4}$	(6.87×10^{-8})
(film)	2.4	7.00×10^{-15}	$\sim 1.8 \times 10^{-11}$		2.3×10^{-8}		5.8×10^{-8}	~ 1.13		0.0027	(3.26×10^{-8})
	3.5	1.75×10^{-12}	1.00×10^{-9}		8.80×10^{-8}		4.5×10^{-8}	1.05		0.0020	(4.71×10^{-8})
	4.6	6.34×10^{-11}	1.40×10^{-8}		2.00×10^{-7}		4.0×10^{-8}	1.06		0.0017	(6.88×10^{-8})
	5.15	2.20×10^{-10}	3.50×10^{-8}		2.67×10^{-7}		4.0×10^{-8}	1.19		0.0024	(13.1×10^{-8})
	7	4.53×10^{-9}	2.00×10^{-7}		5.20×10^{-7}		1.8×10^{-8}	0.83		0.0024	(14.7×10^{-8})
3	9	3.29×10^{-8}	9.19×10^{-7}		7.84×10^{-7}		3.0×10^{-9}	0.56		0.0045	(4.96×10^{-8})
	11	1.50×10^{-7}	1.54×10^{-6}		1.84×10^{-6}			0.56		0.0053	
	14.3	9.00×10^{-7}	5.83×10^{-6}		2.59×10^{-6}			0.73		0.0079	
	20.2	7.47×10^{-6}	2.48×10^{-5}		3.09×10^{-7}			0.86		0.0105	
4	20.2	1.30×10^{-3}	3.01×10^{-2}		1.03×10^{-2}			0.94		0.0014	
5	20	4.70×10^{-7}	5.23×10^{-7}					1.10			

remains constant for small fields and then starts increasing with increase in field. The value of the field at which conductivity starts deviating from its linear value σ_o is the onset field F_o. A criterion to determine the latter is discussed below. With further increase in the bias, the conductivity continues to increase monotonically. As temperature is decreased, σ_o decreases and the sample seems to become nonlinear at a field greater than the one required at a higher temperature; that is, F_o *increases* with decreasing temperature. This behavior is opposite to those found in other two systems (Figs. 4 and 6). Data at each temperature were fitted to the GM expression Eq. (12) containing terms up to $n = 5$. Fits were reasonably good up to $\sigma/\sigma_o \sim 2.5$ and are shown in Fig. 2 (solid lines). However, as seen particularly at $T = 150$ and 195 K, conductivity increased faster than the fitted curves at higher bias and could not be accounted for even by including a $n = 7$ term. This may be related to incipient negative differential conductance regime, as is evident in similar data in Fig. 2c of Ref. 23. Surprisingly, nonlinear least-squares fittings at all temperatures led to either very small or negative values for coefficients of even terms (i.e., $n = 2, 4$) so that the final fittings were done using only three terms: $\sigma(V) = \sigma_o + \sigma_3 V^{5/2} + \sigma_5 V^{14/3}$. Fitted values of the coefficients are given in Table II.

Figure 3 shows the result of making the data in Fig. 2 collapse into a single curve by suitable scaling. It is convenient to start with a temperature such that the data at that temperature are predominantly Ohmic but contain minimum non-Ohmic regime. In the present case the appropriate starting temperature is 80 K. The conductivity was scaled by its Ohmic values σ_o. For the field, any arbitrary choice (e.g., 1) for F_o would do as far as data collapse is concerned. For the next higher temperature, the conductivity was scaled as before but F_o was adjusted in such a way that this set of data merged with the earlier one as well as possible. The same procedure was then repeated for all the other temperatures in increasing order. Note that in this method F_o is determined only up to a constant value. Multiplying all F_o's by a constant only shifts the merged curve along the field axis without altering the curve anyway. To facilitate comparison, and for F_o to be interpreted as an onset field, its scale was fixed by adopting a uniform criterion that the conductivity at the onset field would be double of its Ohmic value; that is, $\sigma(F_o) = 2\sigma(0) = 2\sigma_o$. The excellent data collapse up to about $\sigma/\sigma_o \approx 3$ seen in Fig. 3 proves the existence of a field scale at each temperature. F_o thus obtained following the above criterion is plotted with log-log axes as a function of both temperature T (solid symbols) and the corresponding σ_o (open symbols) in the inset. The solid line indicates a power law $F_o \sim \sigma_o^{x_T}$ with an exponent x_T being equal to -0.329 ± 0.014, which is negative, as suggested by the orientation of the dotted line in Fig. 1. However, no such relation is apparent in the functional dependence on T. Results thus validate the scaling as given in Eqs. (4) and (5). Since all

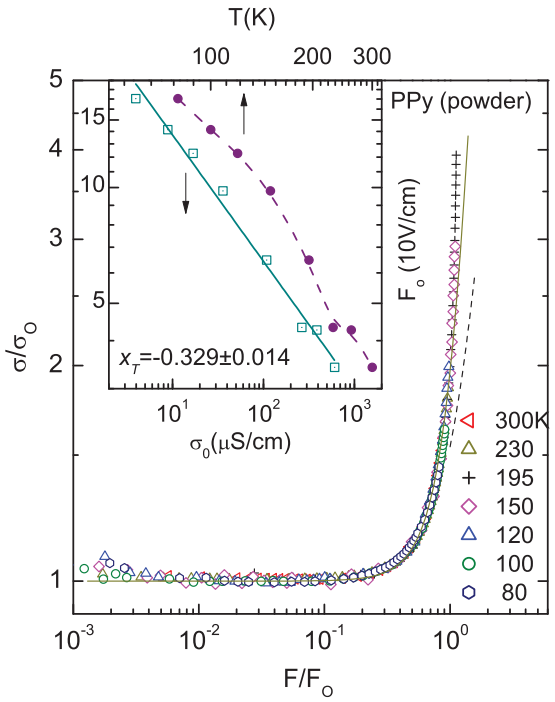

FIG. 3. (Color online) Scaling of the same data as in Fig. 2 to achieve data collapse as shown. The scale of the onset field F_o is fixed by adopting a common criterion $\sigma(F_o) = 2\sigma_o$ in this paper. The solid line is a fit to the scaled version Eq. (15) of GM expression with only two odd ($n = 3, 5$) nonlinear terms: $\sigma/\sigma_o = 1 + 0.54q^{5/2} + 0.42q^{14/3}$ ($q = F/F_o$). The dashed line is a plot of the same expression up to the $n = 3$ term only. The inset shows two log-log plots of F_o vs σ_o (open symbols) and T (solid symbols). The solid line is a linear fit to the data with a slope x_T as shown.

the curves in Fig. 2 that were fitted by the GM expression also collapse on to a single curve, it is expected that the latter would also be fitted by the scaled form Eq. (15). This is indeed confirmed by the solid line in Fig. 3, which is a fit according to $\sigma/\sigma_o = 1 + \bar{c}_3 q^{5/2} + \bar{c}_5 q^{14/3}$ with $\bar{c}_3 = 0.54$ and $\bar{c}_5 = 0.42$. The relative high value of $\bar{c}_5$ confirms the rapid increase of the conductivity with field. A plot (dashed line) of the same fitting expression without the $n = 5$ term is also shown to highlight the contribution of the higher nonlinear term. The divergence of the data from the fitted curves at higher fields ($\sigma/\sigma_o \approx 3$) as seen in the figure is due to the negative differential conductance as discussed above. $\bar{c}_n$'s in the fitting expression are simply averages of c_n's, calculated at each temperature from Eq. (14) using σ_n's and $V_o = 0.1F_o$ (thickness being 0.1 cm), and given in Table II (for calculation of $\bar{c}_5$, data at 80 K and 100 K were ignored as non-Ohmic regimes were small). The highest nonlinear term in the fitting expression depends upon the maximum value of the measured normalized conductivity, $(\sigma/\sigma_o)_{\max}$, which is about 4 in the present case. Notice that $\bar{c}_3 + \bar{c}_5 = 0.96$, close to 1 as expected from Eq. (16) by applying the criterion for F_o. The deviation of the sum of $\bar{c}_n$'s from 1 should be an indicator of how well the criterion for the field scale was implemented during scaling and quality of overall scaling.

It may be mentioned here that if one is interested only in the nonlinearity exponent but not the scaling function, it could be

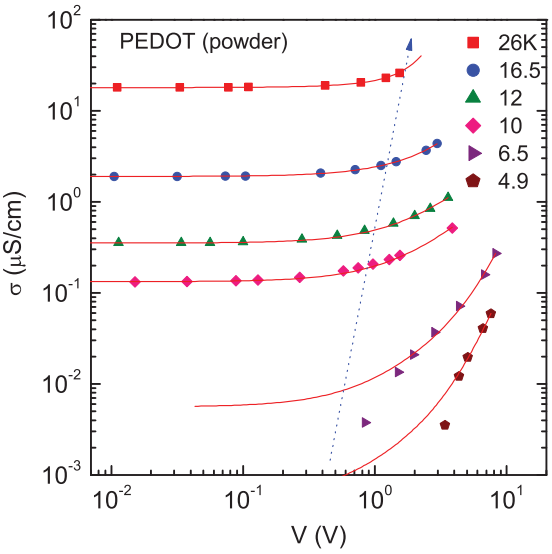

FIG. 4. (Color online) Variation of conductivity vs electric field in doped PEDOT (sample 2) at different temperatures as indicated. The dotted line schematically indicates the movement of the onset bias with increasing temperature. The solid lines are fits to the GM expression Eq. (12). See text for details.

obtained from experimental data by another method used by Gefen *et al.*[44] for characterizing the crossover to the nonlinear regime in a percolating system. In this method, one defines the crossover field F_o such that the conductance at this field deviates by an arbitrarily chosen factor ϵ from its zero-field value; that is, $\Sigma(F_o) = \Sigma_o(1 + \epsilon)$. Obviously, the value of the exponent should not depend upon the choice of ϵ as verified in discontinuous gold films.[44] $\epsilon = 1$ coincides with the criterion adopted in this paper. Clearly, this method will work as long as Σ_o can be obtained from data. However, particularly at low temperatures, Ohmic conductivities become too small to be above the noise floor of measurements and measurements are feasible only in highly nonlinear regimes. Consequently, Σ_o's cannot be obtained directly from the data. In such cases, the method of scaling provides an alternative way to take into account such nonlinear data as illustrated in the cases discussed next.

B. PEDOT (powder)

The field dependence of dc conductivity σ of a PEDOT (powder) system at different temperatures ranging from 4.9 K to 26 K are shown in Fig. 4. The nonlinear response of conductivity to the application of electric field can be clearly seen from the figure. The sample had an Ohmic conductance Σ_0 of 0.026 S at room temperature. It is observed from the figure that the dotted line points right, in contrast to the behavior in the previous case; that is, the onset field F_o *increases* with increasing temperature or conductivity. In fact, the overall shape of the curves are somewhat divergent with bias in PPy (powder) (Fig. 2) but in contrast, appear convergent in PEDOT (powder) (Fig. 4). The converging feature naturally indicates eventual temperature independence of conductivity at large fields. As before, data at each temperature were fitted to the GM expression Eq. (12) containing terms up to $n = 5$.

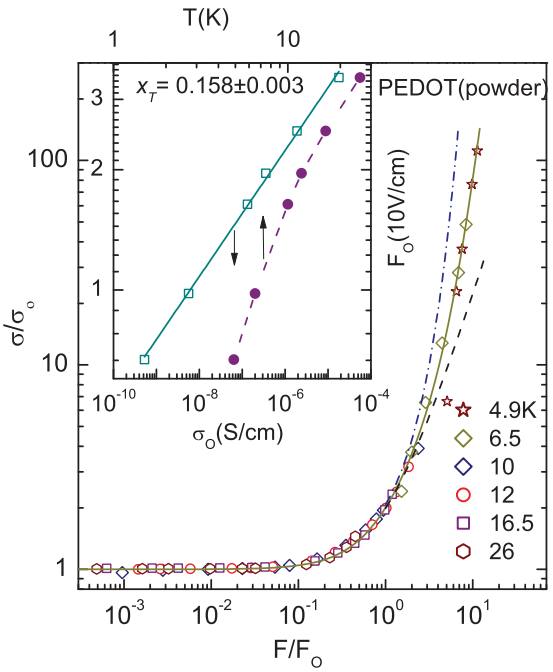

FIG. 5. (Color online) Scaling of the same data as in Fig. 4 to achieve data collapse as shown. The solid line is a fit to Eq. (15) with only even ($n = 2$, 4) nonlinear terms: $\sigma/\sigma_o = 1 + 0.92q^{4/3} + 0.011q^{18/5}$ ($q = F/F_o$). The dashed line is a plot of the same expression up to the $n = 2$ term only. The dash-dotted line is a fit to an exponential function Eq. (9). The inset shows two log-log plots of the scaling field, F_o vs σ_o (open symbols) and T (solid symbols). The solid line is a linear fit to the data (open symbols) with slope as shown.

In this case, the least-squares method at all temperatures led to either very small or negative values for coefficients of odd terms (i.e., $n = 3$, 5) so that the final fittings were done using only three terms: $\sigma(V) = \sigma_o + \sigma_2 V^{4/3} + \sigma_4 V^{18/5}$. The Ohmic conductivities at 4.9 K and 6.5 K were obtained from the extrapolated line, $\ln\sigma_o$ vs $T^{-0.5}$ in Fig. 1. The bias ranges at 10 K and 12 K were too limited to yield reliable values for c_4's. Fits (solid lines in Fig. 4) are seen to be excellent. Fitted values of the coefficients are given in Table II.

All the curves in the figure, starting with the one at 26 K and using the same criterion for F_o as in the previous case, could be made to collapse into a single curve as shown in Fig. 5. Since the data for $T < 7$ K have no linear region, the method in Ref. 44 for determining the exponent cannot be applied. For scaling purpose, extrapolated σ_o's were used. However, when conductivities at these low temperatures are scaled with these σ_o's, the scaled data were all larger than the rest of data at higher temperatures. Absence of any overlapping data sets introduce uncertainty in the choice of F_o. The larger the gap between data sets is, the higher the margin of error is. However, the margin of error may be considerably reduced when, as in the present case, the collapsed curve is compared in a somewhat self-consistent manner to some function it is expected to follow. The solid line in the figure is an excellent fit to $\sigma/\sigma_o = 1 + \bar{c}_2 q^{4/3} + \bar{c}_4 q^{18/5}$ with $\bar{c}_2 = 0.99$ and $\bar{c}_4 = 0.015$ so that $\bar{c}_2 + \bar{c}_4 = 1.005 \approx 1$, as expected. $\bar{c}_2$ is the average of c_2's (with data at $T = 26$ K ignored), whereas $\bar{c}_4$ is consistent with the values of limited number of c_4's. A plot (dashed line) with only $n = 2$ term is also shown to highlight the contribution of the higher nonlinear term, which, as seen, is quite significant in this case, although $\bar{c}_4$ is quite small compared to $\bar{c}_2$. Note that $(\sigma/\sigma_o)_{\max}$ is about 100 compared to 4 in the previous case. The inset shows log-log plots of F_o vs temperature T (solid symbols) and the corresponding σ_o (open symbols). The solid line through open symbols indicates a power law with an exponent of 0.158 ± 0.003. The exponent has a positive value in accordance with the orientation of the dotted line in Fig. 4. No reasonable straight line could be drawn through solid symbols.

C. Polypyrrole (film)

Two sets of field-dependent conductivities of PPy films are presented in Fig. 6. Panel (a) shows data taken in sample 3 at different temperatures as marked and is similar to Figs. 2 and 4, whereas panel (b) shows data at $T \approx 20$ K taken in three different samples as indicated. In the former, the initial conductance changed due to change in the temperature, whereas in the latter, the same was achieved by having different quenched disorder in the samples. As seen in the Figs. 2 and 6, the basic qualitative response to the electric field is similar in all the PPy samples irrespective of structure (i.e., powder or film) or sample condition in that at any temperature the conductivity increases monotonically with the field, starting from a constant value at small bias. However, a closer look reveals subtle differences as illustrated by the orientations of the schematic lines which indicate the movement of the onset field F_o with increasing linear conductivity. In Fig. 6(a), the line points right (i.e., F_o *increases* with the linear conductivity), as in Fig. 4, whereas in Fig. 6(b), it points left (i.e., F_o *decreases* with the linear conductivity), as in powder (Fig. 2). Note that although both panels have one common set of data (sample 3 at $T = 20$ K) this did not prevent two sets of data with two different driving variables—namely, temperature and disorder—from exhibiting opposite behavior in the onset field F_o. As mentioned in the previous case, the relation of the overall shape of the curves with the orientation of the dotted lines is now clearly seen in the two panels—the left one showing a convergent behavior as in Fig. 4 and the right one a divergent behavior as in Fig. 2—in the *same* system. At the low temperatures (2 K–5 K) conductivity indeed become nearly independent of temperature at large biases as seen in panel (a), a feature that was strongly hinted at in the data of PEDOT. As before, data at each temperature or disorder were fitted to the GM expression Eq. (12) containing terms up to $n = 6$. In this case, the least-squares method at all temperatures led to either very small or negative values for coefficients of odd terms (i.e., $n = 3$, 5) so that final fittings were done using only four terms: $\sigma(V) = \sigma_o + \sigma_2 V^{4/3} + \sigma_4 V^{18/5} + \sigma_6 V^{40/7}$. Fittings to data at $T \leqslant 7$ K used the Ohmic conductivities obtained from extrapolation of $\ln\sigma_o$ vs $T^{-0.5}$ line. Note that the temperature independence at low temperatures is also apparent from roughly the same values of σ_6 (see Table II).

Figure 7 shows scaling of the data in the two panels of Fig. 6. There are two curves showing data collapse: one (labeled **b**) belongs to different samples in panel (b) and another (labeled **a**) belongs to the sample 3 at different temperatures

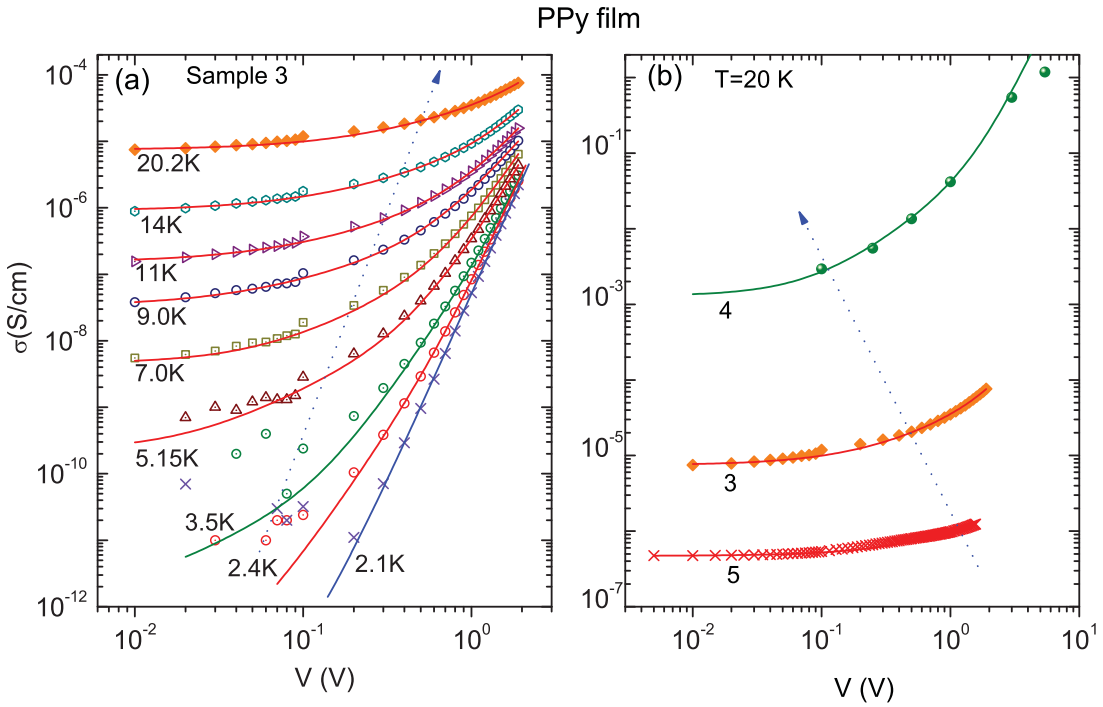

FIG. 6. (Color online) (a) Variation of conductivity vs field in a doped PPy film (sample 3) at different temperatures as indicated. The dotted line schematically indicates the movement of the onset field with increasing temperature. The solid lines are fits to the GM expression Eq. (12) with parameters given in Table II. (b) Similar data as on the left panel taken at the same temperature 20 K in three different samples as indicated with different quenched disorder. The dotted line schematically indicates the movement of the onset bias with increasing conductivity. The solid lines are fits using the GM model. See text for details. Note that the data represented by solid diamonds in both panels are the same.

in panel (a). Data collapse has been achieved by following the same procedure as adopted in previous cases including the criterion for fixing the onset field F_o, namely, $\sigma(F_o) = 2\sigma_o$. Excellent data collapses are seen to have been achieved in both cases, with curve **a** covering nine orders of magnitude in conductivity and five orders in field. The data of curve **b** have been shifted upward for clarity. Moreover, lines, instead of symbols, are used in this case to highlight the quality of data collapse. In case of curve **a**, extrapolated σ_o's were used for scaling particularly at low temperatures. The solid lines in the figure are excellent fits to $\sigma/\sigma_o = 1 + \bar{c}_2 q^{4/3} + \bar{c}_4 q^{18/5} + \bar{c}_6 q^{40/7}$. The coefficients $\bar{c}_2$, $\bar{c}_4$, and $\bar{c}_6$ are 0.98, 0.0024, and 6.5×10^{-8} for curve **a** and 0.97, 0.0013, and 0 for curve **b**. In both cases, $\bar{c}_2 + \bar{c}_4 + \bar{c}_6 \approx 1$, as expected from Eq. (16). $\bar{c}_2$'s are same as the average of c_2's in Table II (with data at $T = 2.1$ K ignored), whereas $\bar{c}_4$'s are consistent with the values of limited number of available c_4's. As with PEDOT, the values of $\bar{c}_2$'s are much greater than those of other coefficients although the latter's contributions are significant, as indicated by the dashed and dotted lines. The latter are plots with up to $n = 2$ (dashed) and 4 (dotted) terms only. This is, of course, partly due to the criterion adopted for F_o. Note that $(\sigma/\sigma_o)_{\max}$ is about 10^9 (curve **a**) compared to 100 and 4 in the previous cases. The inset shows log-log plots of F_o thus obtained from scaling as function of both temperature T (solid symbols, curve **a**) and the corresponding σ_o (open symbols, curve **a**; crosses, curve **b**). The solid line verifies the power law Eq. (5) with the exponent $x_T = 0.228 \pm 0.008$. No reasonable straight line could be drawn through the plot of F_o vs T (solid symbols). In case of scaling with disorder, there are only three points that yield a tentative value of the exponent $x_D \sim -0.30$ (the subscript stands for disorder). As expected from Fig. 6, x_D compared to x_T has a negative sign.

D. Other systems in literatures

Nonlinearity exponents x_T in the three systems discussed above are shown in Table III. The latter also contains, for the sake of comparison, results from digitized data of three other CP systems available in literatures. All these systems invariably exhibit the property of scaling Eq. (4). The systems include a *p*-toluensulfonate (PTS)-doped PPy (PPy(R)) film,[23] PTS-doped polydiacetylene (PDA) single crystal[24] and iodine-doped PA nanofiber.[31] The PPy(R) film (0.1–0.15 mm thickness) was obtained by electrodeposition at the current density of 0.2 mA/cm^{-2}. The scaled curve of conductivities at four temperatures (16 K–31 K) in this film looked very similar to that in Fig. 3. It also yielded a negative exponent, -0.16 compared to -0.33 obtained in PPy (powder). The temperature-variation of the Ohmic conductivity of this system has been mentioned in the Introduction.

PTS-doped PDA crystals are quasi-one-dimensional in nature, consisting of weakly coupled linear parallel chains of covalently bonded carbon atoms. It follows a VRH-type conduction ($m = 0.65$–0.70, $T_o = 2570$ K) at low temperatures with a crossover at about 50 K to activated conduction at higher temperatures. Five temperatures between 50 K and 14 K were used such that corresponding data could be digitized with some reasonable accuracy from linear current-field plots (viz. Fig. 7 of Ref. 24) which, particularly at low bias,

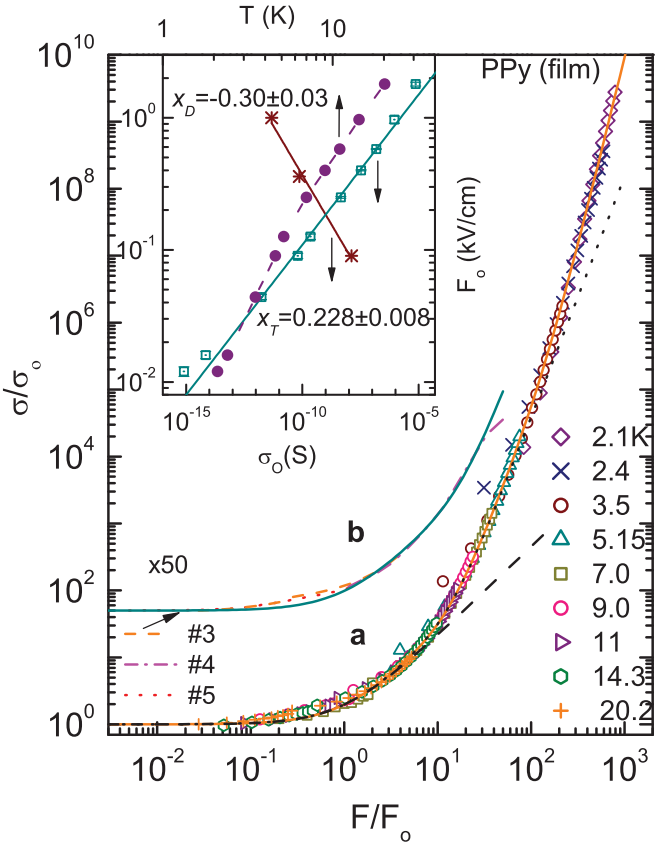

FIG. 7. (Color online) Scaled conductivity σ/σ_o vs scaled field F/F_o of doped PPy films in the two panels of Fig. 6. The scaled data **b** (lines) belonging to different samples are shifted upward for clarity. The solid line is a fit to Eq. (15) with only two even ($n = 2$, 4) nonlinear terms: $\sigma/\sigma_o = 1 + 0.97q^{4/3} + 0.0013q^{18/5}$ ($q = F/F_o$). The scaled data **a** with symbols belong to different temperatures. The solid line through it is a fit to the GM expression Eq. (15) with three even ($n = 2, 4, 6$) nonlinear terms: $\sigma/\sigma_o = 1 + 0.97q^{4/3} + 0.0024q^{18/5} + 6.5 \times 10^{-8}q^{40/7}$. The dashed line is a plot of the same expression but with terms up to $n = 2$ only. Similarly, the dotted line is a plot with terms up to $n = 4$ only. The inset shows three log-log plots of F_o vs σ_o (open symbols and crosses) and T (solid symbols). The crossed symbols, belonging to three different samples, have been appropriately shifted ($\times 10^{-5}$, $\times 0.2$) to be within the scales as shown. The solid lines are linear fits to the data with slopes x_T (open symbols) and x_D (crosses) as shown.

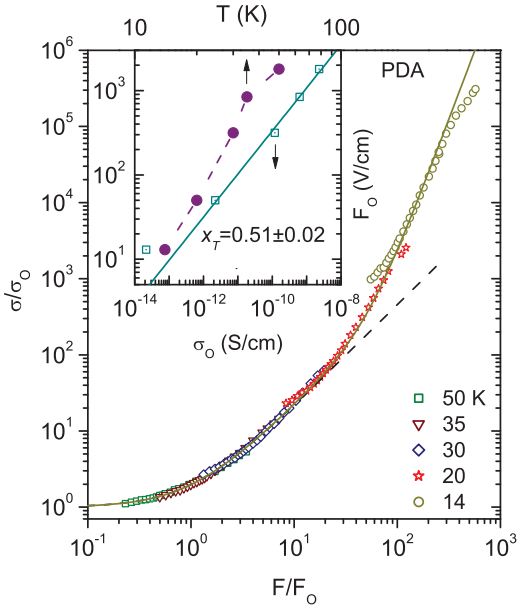

FIG. 8. (Color online) Scaling of the data in a PDA single crystal from Ref. 24 to achieve data collapse as shown. The solid line is a fit to Eq. (15) with only even ($n = 2$, 4) nonlinear terms: $\sigma/\sigma_o = 1 + 0.98q^{4/3} + 0.000\,123q^{18/5}$ ($q = F/F_o$). The dashed line is a plot of the same expression without the $n = 4$ term. The inset shows two log-log plots of the scaling field, F_o vs σ_o (open symbols) and T (solid symbols). The solid line is a linear fit to the data (open symbols) with slope, as shown.

are more prone to digitizing errors than conductivity-field ones. Nonetheless, Fig. 8 shows clear evidence of scaling in conductivities at different temperatures covering nearly six decades in conductivity and four decades in field. The solid line in the figure is an excellent fit over the whole range to $\sigma/\sigma_o = 1 + \bar{c}_2 q^{4/3} + \bar{c}_4 q^{18/5}$. The coefficients $\bar{c}_2$ and $\bar{c}_4$ were 0.98 and 1.23×10^{-4}, respectively, and add up to nearly 1, as expected. These values were consistent with the coefficients obtained from fittings of data at each temperature to the GM expression Eq. (12). The dashed curve is a plot with up to $n = 2$ term only. It was found that the fitted values of σ_o's (also used in scaling) were progressively less than those given in the paper with decreasing temperature, by as much as an order of magnitude at 20 K. $(\sigma/\sigma_o)_{\max}$ is about 10^5 compared to 10^9 in PPy film (this work). The nonlinearity exponent was $x_T = 0.51 \pm 0.02$. It is seen in Fig. 8 that curves particularly at lower temperatures tend to rise less rapidly at higher fields than at lower ones. This is because those portions of the curves follow $F^{-1/2}$ dependence Eq. (11) and are outside of the scaling domain.[40] In fact, the collapsed curve really represents an envelope of all scaled curves at different temperatures. Such $F^{-1/2}$ dependence in PPy film of this work was insignificant (see Fig. 7), although both these systems had the VRH exponent m equal to 1/2.

Individual iodine-doped PA nanofibers of diameters 10-40 nm were different from other systems discussed so far in that the Ohmic conductance exhibited an activated-type rather than VRH conduction. At low temperatures below 30 K, the I-V characteristics were reported to follow the Zener-type tunneling, $\Sigma = \Sigma_o \exp(-F_u/F)$, where F_u in the argument depends on the magnitude of the energy gap and the effective mass of tunneling electrons.[29] The I-V curves were non-Ohmic and temperature independent up to 30 K, above which I-V curves were temperature dependent. Upon comparing with Eq. (11) it becomes evident that the above equation really characterizes the high-field regime that becomes apparent particularly at low temperatures (see also Fig. 6) and is not compatible with the scaling Eq. (4). In fact, I-V curves again exhibit the same scaling behavior shown in Fig. 9 as in other cases discussed here. I-V data were obtained in a single iodine-doped PA nanofiber of diameter 20 nm at various temperatures (Fig. 1 of Ref. 31). Of those, data at five temperatures (234 K–103 K) were found suitable for digitization and presented in the scaled form in Fig. 9. In spite of inherent noise in the data, high quality of data collapse

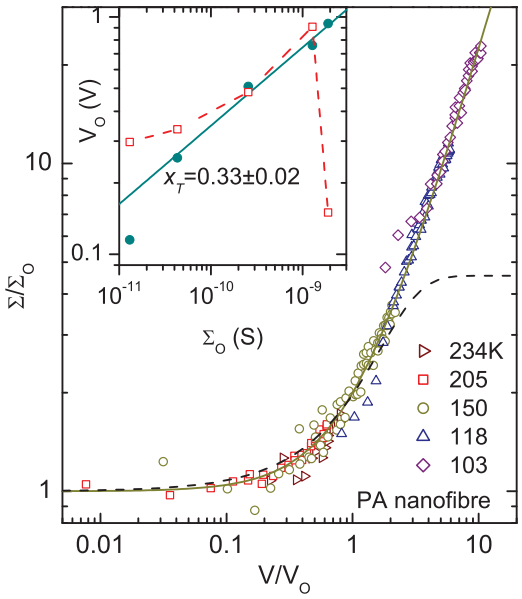

FIG. 9. (Color online) Scaling of the data in a PA nanofiber from Ref. 31 to achieve data collapse as shown. The solid line is a fit to the GM expression Eq. (15): $\sigma/\sigma_o = 1 + (V/V_O)^{4/3}$. The dashed line is a plot of the expression Eq. (22) with $h = 0.21$. Inset shows two log-log plots of the scaling bias V_o vs Σ_o. One set of data (open symbols) is obtained from fittings to Eq. (22) and another set (solid symbols) from scaling. The solid line is a linear fit to the data (solid symbols) with slope as shown.

is quite evident. The solid line in the figure represents an excellent fit to $\sigma/\sigma_o = 1 + q^{4/3}$, thus requiring only a $n = 2$ term in the GM expression. Authors[31] fitted the I-V curves to the following expression:

$$\sigma = \frac{\sigma_0 \exp(V/V_o)}{1 + h\,[\exp(V/V_o) - 1]}, \tag{22}$$

where σ_o is the Ohmic conductivity and the parameter $h = \sigma_o/\sigma_\infty$ ($h \leqslant 1$), σ_∞ being the value of σ at large voltages V. V_o is a voltage scale factor. The dashed curve in Fig. 9 is a plot according to Eq. (22) with $h = 0.21$. The particular value of h was chosen to satisfy the criterion for the bias scale, $\Sigma(V_o) = 2\Sigma_o$. The fit runs above the data for $V/V_o < 1$, and runs below the data for $V/V_o > 1$. Moreover, the variation in h with temperature and the saturation at large bias clearly reveals inadequacies of the above expression in describing the field-dependent conductance. Discrepancies at low bias between experiments and Eq. (22) were already noted.[33] The inset shows two plots of V_o vs Σ_o with one set of V_o's (solid symbols) obtained from scaling and another set of V_o's (open symbols) obtained from fittings to Eq. (22). Comparison of the two sets shows further limitations of the above expression. The nonlinearity exponent was determined to be $x_T = 0.33 \pm 0.02$.

V. DISCUSSIONS

The last section dealt with four different CP systems, namely, PPy, PEDOT, PDA, and PA in as many forms, namely powder, film, crystal, and nanofiber. Even under such diverse conditions, the scaling phenomena as embodied in Eq. (4) and demonstrated in Figs. 3, 5, 7, 8, and 9 stand validated in a clear and unambiguous manner. Furthermore, the figures also confirm the remarkable fact that there exists a *single* field scale in any given sample at least within the experimental ranges of field and conductivity spanning more than five and nine orders of magnitude, respectively. This is contrary to the predictions in the field-dependent VRH theories discussed in Sec. II. Thus, an important objective of this paper, as stated in the introductory section, is fulfilled. We believe that the scaling phenomena observed in CPs here, and in amorphous- and doped-semiconductors[40] earlier, thus indicate a general and fundamental property of the class of disordered systems with localized states. The scaling analysis here follows that of critical phenomena in thermodynamic phase transitions[43] and, hence, the method of analysis described in Sec. III naturally differs from that hitherto adopted, for example, in Refs. 24,25, and 46. The method, in absence of a proper theory, is primarily phenomenological but yields a concrete number—the nonlinearity exponent—as a characterization of the underlying conduction mechanism. The fact that the nonlinearity exponent can have both positive and negative values illustrates subtle features hitherto unnoticed in non-Ohmic conduction in disordered systems. Let us now consider details of scaling, namely, the scaling variables (which F_o depends on) and scaling function, Φ, and their possible connections to the microscopic picture.

A. Field scale F_o and scaling variable

To start with, let us note that at low fields CP systems exhibit some sort of thermally activated conduction as described by Eq. (1), with m ranging from 1/4 to 1. VRH is actually a phonon-activated hopping between localized states irrespective of the presence or absence of polarons. Discussed in Sec. II, traditional theories incorporating field effects in VRH conduction have a number of predictions or implications which are at variance with experimental results.

First, two field scales F_o and F_u (corresponding to the two length scales, the hopping length R_h and localization radius a, respectively) are predicted, whereas only one scale is experimentally observed. Second, the scale F_o is basically set by temperature and supposed to vary as $F_o \sim T^\alpha$ Eq. (10), where $\alpha = 1 + m\mu$ is a positive number and always greater than 1. However, log-log plots of F_o vs T (insets in Figs. 3, 5, 7, and 8) generally deviate from linearity to varying degrees. They seem to be better described by two power laws with two exponents: α_1 at low temperatures and α_2 at higher temperatures with $\alpha_1 \geqslant \alpha_2$. Nonetheless, if the data in the insets are still subjected to linear fits, slopes (i.e., α's) turned out to be 0.98, 2.24, and 4.1[53] in PEDOT, PPy (film), and PDA, respectively, compared to predicted values of 1.5(2), 1.5(2), and 1.68(2.36) for $\mu = 1(2)$, respectively. Third, the problem of temperature directly determining the field scale is rather dramatically highlighted by the measurements in three samples of PPy film [Fig. 6(b)] at a temperature of 20 K, each one having a different quenched microscopic disorder and characterized by the Ohmic conductivity σ_o. If F_o is indeed set by temperature alone, it should have been basically same for each sample in the figure as measurements were performed at the same temperature. However, the inset in Fig. 7 clearly shows that F_o varies with σ_o and, within

TABLE III. Comparison of nonlinearity exponents x_M obtained using scaling and extended GM analysis Eq. (20) in various CP systems. M stands for the variable used to vary σ_o: T, temperature; D, disorder; and B, magnetic field. y_n is given by $\sigma_n \sim \sigma_0^{y_n}$ with values of σ_n's of some samples displayed in Table II. Note that quoted errors do not include the errors in data collapse processes, which could be up to 10%.

System	M	x_M scaling	x_M GM ($n = 2/3$)	y_2	y_3	x_M GM ($n = 4/5$)	y_4	y_5	y_6
PPy (powder)	T	-0.329 ± 0.014	-0.31 ± 0.03		1.78 ± 0.08	-0.36 ± 0.03		2.67 ± 0.13	
PPy (film)[23]	T	-0.155 ± 0.012	-0.13 ± 0.02		1.32 ± 0.04				
PPy (film)	T	0.228 ± 0.008	0.230 ± 0.003	0.693 ± 0.004		0.21 ± 0.01	0.25 ± 0.01		~ 0
PPy (film)	D	~ -0.3							
PPy (film)	B	0	0	1		0	1		1
PEDOT (powder)	T	0.158 ± 0.003	0.170 ± 0.005	0.774 ± 0.007		~ 0.12	~ 0.57		
PDA (crystal)[24]	T	0.51 ± 0.02	0.49 ± 0.02	0.34 ± 0.02					
PA (nanofiber)[31]	T	0.33 ± 0.02	0.29 ± 0.06	0.62 ± 0.08					

the limited range, is compatible with Eq. (5), albeit with a different nonlinearity exponent. It proves that a field scale is an intrinsic property of a disordered sample but could be modified by various other parameters such as temperature, etc. Significance of the role of disorder becomes further apparent when compared with the results obtained by Bufon *et al.*[25] from measurements at different magnetic fields. Figure 11 displays σ-V curves (dashed) at three magnetic fields B, as indicated. The conductivity generally decreases with increasing magnetic field. It is found that the three curves could be made to collapse into a single curve (solid) by simply scaling the conductivity at each magnetic field by a factor λ (arbitrary up to a constant factor), as shown. The bias did not need any scaling. This means that the field scale was independent of B unlike disorder, and consequently, the corresponding nonlinearity exponent x_B is 0. Fourth, in some systems such as PPy (powder) (inset of Fig. 3) and PPy(R) film (Table III), α (as well as the nonlinearity exponent x_T) is negative. This is a serious disagreement as it is irreconcilable with the theories.

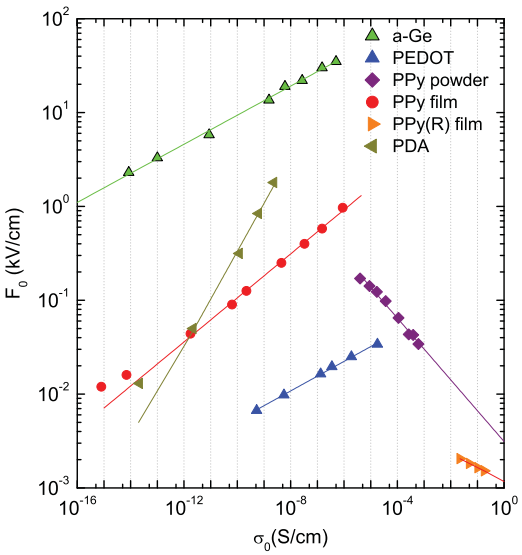

FIG. 10. (Color online) Field scale vs linear conductivity in various systems. The plot for a-Ge is from Ref. 40. The data of PPy(R) film have been shifted to the left by a factor of 10^4.

In contrast, log-log plots of F_o vs σ_o are consistently linear, as seen in Figs. 9 and 10, the latter displaying data from different CP systems (Figs. 3, 5, 7, and 8), including PPy(R) in the same scales (PA nanofiber is excluded because of variables with different units). Linearities in the plots give credence to the empirical power law $F_o \sim {\sigma_o}^{x_T}$ Eq. (5), which is radically different from Eq. (9) in that the variable in the power law is not the temperature itself but the linear conductivity σ_o, which is, of course, a function of temperature. All these considerations suggest that σ_o should be considered as the appropriate scaling variable in Eq. (4), which then reads as

$$\sigma(M,F)/\sigma_o = \Phi(F{\sigma_o}^{-x_M}), \tag{23}$$

where M stands for the variable(s) used to vary $\sigma_o = \sigma(M, F = 0)$. Equation (23) allows description of the scaling of the field-dependent conduction along various paths in the variable space in a natural fashion without any obvious contradiction. In analogy with the scaling formulation of thermodynamic critical phenomena,[43] $\sigma_o = 0$ defines a "critical" point. The Ohmic conductivity σ_o plays the traditional role of temperature T in that it sets the field scale, which, in turn, is expected to correspond to some physical length scale. The latter is yet to be explained but must be distinct from either a or R_h.

While allowing a view of data in six samples at a glance, Fig. 10 also provides a basis for quantitative comparison of the field scales across those systems and amorphous germanium (a-Ge)[40] included for reference. The comparison, of course, is not straightforward as the slopes x_T have different values. However, it is seen that CP systems are generally electrically "soft" compared to a-Ge since the onset field in a CP system is smaller than that in a-Ge in the displayed range of conductivity. For a quantitative comparison, let us consider a-Ge and PEDOT since both systems have nearly same slope (nonlinearity exponent) of 0.16. The prefactor A_T in Eq. (5) which represents the strength of a field scale is 331 and 0.2 $(\mathrm{kV/cm})(\mathrm{S/cm})^{-0.16}$, respectively, that is, the onset field in a-Ge is roughly 1600 times that in PEDOT. Now, simple dimensional considerations lead to an expanded expression for F_o:

$$F_o \propto \frac{k_B T_o}{ea}\left(\frac{ah\sigma_o}{e^2}\right)^{x_T}, \tag{24}$$

where e^2/h is the quantum of conductance and $k_B T_o$ is a characteristic energy scale. From Eqs. (5) and (24) we have $A_T \sim T_o/a$. Taking localization lengths in the two systems to be of same order of magnitudes (∼1 nm) and with $T_o \approx 10^8$ and 1800 in a-Ge and PEDOT, respectively, the ratio $F_o(a\text{-Ge})/F_o(\text{PEDOT})$ is about $\sim 5 \times 10^4$, one order of magnitude greater than 1600. VRH theories fare even worse. According to Eq. (10), $F_o \sim 1/aT_o^{\alpha-1}$ so that the ratio $F_o(a\text{-Ge})/F_o(\text{PEDOT})$ is about $1800^{1/2}/10^{8/4} \sim 1$, three orders of magnitude less than the experimental value.

B. Scaling function Φ

The field-dependent VRH theories[34,36,37] predict a simple exponential Eq. (9) at low and intermediate fields, to which the scaled data of PEDOT (powder) have been fitted for illustration purpose (dash-dotted line in Fig. 5). The fitted curve appears to match data well in the low-field region ($F/F_o \sim 1$) but gradually deviates from it by rising faster in the high-field region. Moreover, as shown in the inset of Fig. 5, F_o fails to follow the temperature-dependence as given by Eq. (10). Such inconsistent behavior of the VRH theory is quite typical. Inadequacies of Eq. (22) in case of PA nanofiber have been discussed earlier in detail (see Fig. 9). Let us now discuss how the GM expression Eq. (12) describes the CP data in various systems.

Fits to the I-V data at different temperatures as well as disorder are shown in Figs. 2, 4, and 6(b), and to the scaled curves in Figs. 3, 5, 7, 8, and 9. The near perfect agreement between the experimental data and the theoretical fits is quite remarkable in view of the range of data covered: more than nine orders of magnitude in conductance and nearly five orders of magnitude in field. Furthermore, fits to the scaled curves using the scaled version of the GM expression Eq. (15) provide absolute justification of the assumption Eq. (14) and underline the relations that exist among the coefficients in the GM expression applied to macroscopic samples but were not foreseen in the theory.[39] The fact that coefficients $\bar{c}_n$'s used in

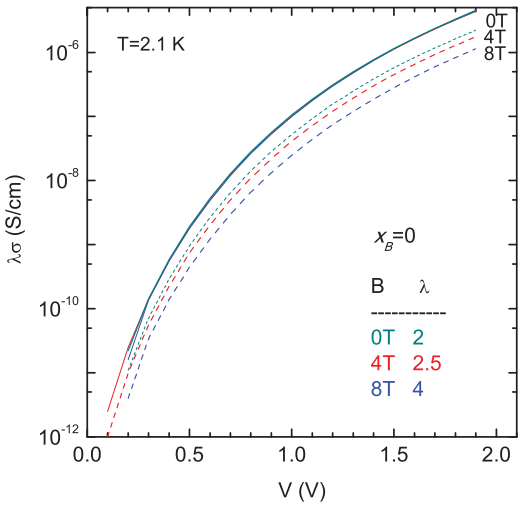

FIG. 11. (Color online) Conductivity vs bias voltage (dashed curves) in the PPy film (sample 3) at three magnetic fields (after Ref. 25). Only conductivity of each curve need to be scaled with a factor λ to collapse onto the solid curve. The nonlinearity exponent x_B is zero.

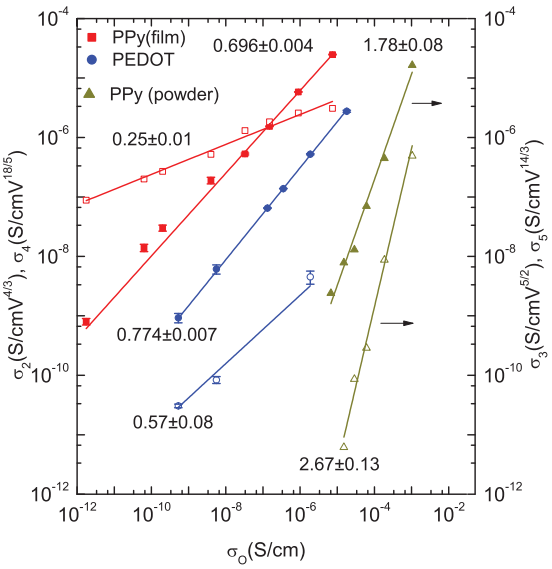

FIG. 12. (Color online) Log-log plots of GM coefficients vs linear conductances. Solid lines are linear fits to the data with slopes as indicated.

the fits to the scaled curves correspond closely (within errors) to c_n's (Table II) obtained from fittings of individual curves also demonstrates those relations in a self-consistent manner. It may be recalled that two assumptions about the coefficients, namely, Eqs. (14) and (18), led to the important expression Eq. (20) for the nonlinearity exponents x_T in the GM model, which allowed a number of conclusions to be drawn on the properties of x_T itself. Fitted values of the coefficients σ_n's Eq. (12) for different values of n given in Table II are plotted against σ_o using log-log scales in Fig. 12. The linearity of the plots amply validate the assumption Eq. (18). While such power-law relations are also predicted in mesoscopic systems Eq. (19), the experimental values seen in Fig. 12 could be significantly different from the predicted ones. Experimental values include numbers larger than the maximum predicted value of 0.67 as in PPy (powder) and PEDOT. However, experimental y_n's (see Table III) do satisfy inequalities in Eq. (21). Furthermore, there is a spectrum of values rather than a single value for a given channel.

A close look at Table II reveals yet another intriguing feature of channel selection: Only the "even" channels (i.e., channels with even number of localized states) appear in the fittings of systems such as PEDOT, PPy film, etc., having positive nonlinearity exponents ($x_T > 0$), whereas only the "odd" channels appear in the fittings of other systems such as PPY (powder) having negative nonlinearity exponent ($x_T < 0$). As a result, the lowest channel contributing to non-Ohmic conduction is a two-impurity channel ($n_o = 2$) in the former, and a three-impurity channel ($n_o = 3$) in the latter. There was no instance of mixing of terms of the two series (i.e., even and odd) in any of the samples investigated here. However, no such selection of channels was detected in a mesoscopic system of metal-amorphous silicon-metal tunnel junctions where all channels from $n = 2$ to 5 were found to be present in some Σ-V curves.[49] In general, the theory does not provide any clue to this phenomena of selection, and in particular, to the properties of

CP systems responsible for this. Similar selection has been also noticed in other hopping systems such as amorphous/doped semiconductors.[40] We also note an opposite trend for PPy films with different quenched disorder [Fig. 6(b)] having a negative nonlinearity exponent where the best fits are obtained with even channels in the GM expression. This is not surprising as one of the curves was earlier part of the data collapse of field-dependent conductances at various temperatures. The nonlinearity exponent was found positive [inset, Fig. 6(a)] and fits to the GM expression consisted of even channels only. Differences between the systems described by even and odd channels can be seen in the values of c_n's in Table II. In case of even channels, c_2's are close to 1 and rest of c_n's are very small. However, in case of odd channels, c_n's are comparable as in PPy (powder).

It is seen from Figs. 5, 7, and 8 that the CPs such as PEDOT, PPy, and PDA were described by the GM expression with only even non-Ohmic channels: $\sigma/\sigma_o = 1 + \bar{c}_2 q^{4/3} + \bar{c}_4 q^{18/5} + \bar{c}_6 q^{40/7}$, where $q = F/F_o$. The data ranges were sufficiently large that each system needed at least two non-Ohmic terms for fitting. While the coefficient $\bar{c}_2$ was close to 1 in all the systems, $\bar{c}_4$ was 0.011, 0.0024, and 0.000 123, respectively. Such decreasing values of $\bar{c}_4$ means decreasing rate of rise of conductivity with field. Another indicator of this trend could be q_4, the value of q in a system above which the fitting (the dashed curve in the corresponding figure) with only the lowest channel ($n = 2$) deviates from the scaling curve. The increasing value of q_4, roughly 2, 10, and 20, respectively, in the three systems does correlate with decreasing $\bar{c}_4$. More significantly, the decreasing $\bar{c}_4$ correlates well with the increasing nonlinearity exponent, which are 0.16, 0.23, and 0.51, respectively (Table III): The smaller the value of a nonlinearity exponent is, the steeper is the conductivity curve (or larger the value of $\bar{c}_4$). This correlation is, in fact, a result of the relation Eq. (6). The higher-order coefficients such as $\bar{c}_6$ are expected to exhibit similar correlation in values. Incidentally, q_4 is given by $\sigma/\sigma_o = 1 + \bar{c}_2 q_4^{p_2}$ from Eq. (15). q_4 may be interpreted to be the onset field for the fourth channel. It may be pertinent to ask whether each distinct value of the nonlinearity exponent constitutes a different universality class with a distinct scaling function. The answer is rather ambiguous at present. Consider two systems with roughly the same nonlinearity exponents: PPy (powder) with $x_T = -0.33$ and PPy (film) with $x_D \approx -0.3$. However, the former is described by a combination of odd channels whereas the latter is described by a combination of even channels. On the other hand, systems such as PPy (film), PEDOT, PDA, and PA (nanofiber) possess distinct nonlinearity exponents but are all described by a combination of even channels. Each combination is, in fact, identified by a unique set of $\bar{c}_n$'s.

It is quite remarkable that only three nonlinear terms were required to describe data in PPy (film) over nine decades. The finite number of terms is consistent with the requirement that the GM series must terminate at some finite n [item (iv) in Sec. II]. The highest term corresponding to $n = 6$ ($p_6 = 5.7$) was necessary to fit the data at high field ($F/F_o \gg 1$), i.e., data at $T \sim 2.1$ K, which is nearly given by a power law [Fig. 6(a)]. Actually, a log-log plot of the data yielded a slope of $z_T = 5.57$ close to 5.7. However, this value of z_T is higher than $1/x_T = 1/0.23 \approx 4.39$, in apparent disagreement with Eq. (6) for $x_T > 0$. The same happens also in PDA, where $z_T(\sim 3.6) > 1/x_T = 2$. The relation Eq. (6) has been routinely observed to hold in amorphous semiconductors.[40] It is to be noted that in both PPy (film) and PDA, F_o at low temperatures lie above the linear fits (Fig. 10). Whether this is indicative of existence of two slopes merits further careful measurements at low temperatures to resolve this issue.

C. Nonlinearity exponent x_M

Nonlinearity exponents are the concrete outcome of the adopted scaling procedure and are displayed in Table III for various CP systems under different conditions. An exponent can be obtained in two ways. One method has been already illustrated in Figs. 3, 5, 7, 8, and 9. This involves collapsing I-V curves gathered at different values of some parameter M (e.g., temperature) on a curve by suitable choices of F_o and σ_o. The exponent is then obtained using Eq. (5). This method is solely based upon the scaling property of the I-V curves and does not require any knowledge of the scaling function. The latter, if available, can be utilized to obtain the exponent in the second method. It has been shown above that GM expressions Eqs. (12) and (15) describe the relevant data in an excellent manner. Therefore, we can use the expression Eq. (20) for obtaining x_M in terms of model parameters, both direct and derived. y_n's are derived from plots such as those shown in Fig. 12. There are as many y_n's as the number of inelastic tunneling channels. According to Eq. (20), each one of them should yield the same x_T as yet another test of consistency in applicability of the GM model to CPs. This seems to be well borne out within errors (Table III) when the contribution from the second channel is large enough to yield reliable values as in PPy (powder) and PPy (film) (this work). Considering the fact that digitization errors are not accounted in the values quoted in case of samples of other works, agreement between values of the exponents obtained using two methods is quite reasonable. In case of measurements at different magnetic fields, since conductivities are related by some constant factors, we have $y_n = 1$ for all n. Equation (20) leads to $x_B = 0$, in agreement with the value from scaling consideration as discussed earlier. Note that x_M's shown in Table III lie between the bounds $-1/2$ and $3/4$ (see the point i).

There are some striking features in the values of the exponent. It can be both positive and negative. The negative values, particularly one of $x_D \sim -0.3$ in PPy (film) are counterintuitive as evident from the following simple argument. The onset field F_o in a sample without any disorder is basically very large. As disorder is introduced, conductance decreases. At the same time, the electrons become increasingly incoherent as well as number of possible paths multiply. This gives rise to non-Ohmic conduction at a finite F_o. In other words, F_o decreases with Σ_o, indicating $x_D > 0$. Clearly, there is no universal exponent for CPs. There is no characteristic exponent even for a given CP. As seen in Table III, the same PPy sample exhibits two different values of the exponent, 0.23 and 0 depending upon the variable M. Three different PPy samples exhibit as many values of the exponent x_T (-0.33, 0.23, and -0.17), both positive and negative. Furthermore, in PPy (film) x_T and x_D are 0.23 and ~ -0.3, respectively in contrast to

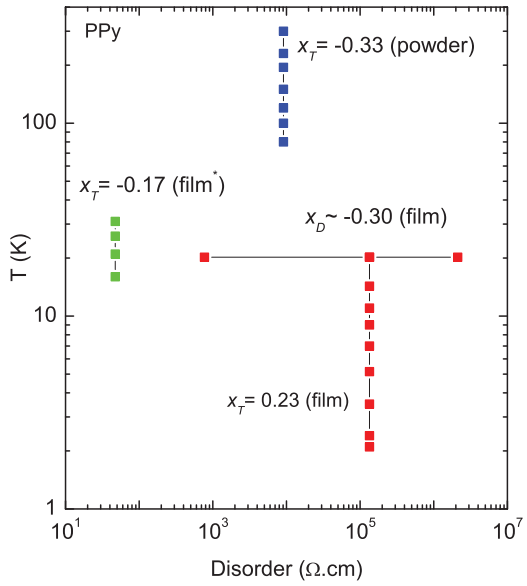

FIG. 13. (Color online) Measurement paths along with associated nonlinearity exponents in various doped PPy samples in the temperature-disorder plane. Disorder here is parametrized by the Ohmic resistivity at 20 K. The data marked with star are from Ref. 23. Note that data from a sample simultaneously belongs to two intersecting lines.

$x_T = x_D \sim 0.45$ in the composite system of carbon-wax.[45,54] This plethora of values could simply indicate that x_M depends upon the path of measurement in the variable space that also includes quenched disorder. Figure 13 illustrates four such paths of measurements in PPy samples along with the corresponding exponents in the temperature-disorder plane. Obviously, unraveling of the details of such dependency in the variable space has to await theoretical understanding of x_M that is lacking at present. In fact, different values of x_M in the same system prove that the hopping network is in both physical as well as energy space, in contrast to the conduction network in composites at room temperature,[55] which is supposed to be purely geometrical in real space. The field scale in CPs cannot be simply determined by geometrical topology of disorder alone. Otherwise, temperature that only provides an energy scale could not have an effect on the scale. This is consistent with result, $x_B = 0$ since magnetic fields do not change either energy levels of charge carriers or disorder and therefore do not warrant a change in the field scale.

D. Final picture and issues with the GM model

Let us consider the broad picture of transport in lightly doped CPs that emerges from the results presented so far and its analysis particularly within the context of the GM model.[39] All the systems considered in this work exhibit an activated-type diffusive transport (including VRH) at low bias, as shown schematically in the top panel of Fig. 14. Such exponential temperature dependence of conductivity is markedly different from power laws, $\sim T^{p_n}$ predicted by the model in the limit $eV \ll kT$. As the applied field is increased beyond the onset value, on one hand the field-dependent conductivities in CPs are described in an excellent fashion by a GM-type expression Eq. (12). This indicates that the transport paths are now in the

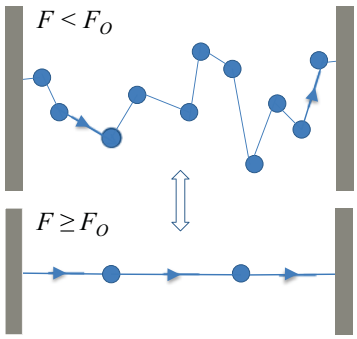

FIG. 14. (Color online) Schematic diagram of possible hopping paths in real space between electrodes for fields (F) less (upper) and more (lower), than an onset field (F_o). The solid circles represent localized states. The lower path corresponds to two-step tunneling, the lowest non-Ohmic channel according to Glatzman-Matveev (Ref. 39). See text for further details.

form of linear chains consisting of multiple localized states, as shown in the bottom panel of Fig. 14. Conduction takes place through inelastic tunneling among those localized states, starting from the lowest two-step tunneling. On the other hand, the fitted parameters (i.e., coefficients σ_n in Table II) are found to possess properties that violate (e.g., temperature dependence in the limit $eV \gg k_B T$) or exceed (e.g., scaling) the originally predicted ones. The justification for application of the GM model to CPs must lie in reconciling these conflicting trends.

Perhaps it is not surprising that there are disagreements between the experimental results in the macroscopic samples used in this work and the predictions of the GM model. The GM -expression Eq. (12) describes transport across a mesoscopic sample of width w of the order of average hopping length; that is, $a \ll w \sim R_h$. A question arises: How do the model predictions change as the bulk limit $w \gg R_h$ is taken? Initially, only a small number of localized states are involved in the dominant hopping process.[49] As the sample dimension or temperature or bias is increased, the optimal n ($n_{\rm opt}$) also increases. Hopping in the limit of large $n_{\rm opt}$ has been discussed by several authors[56,57] and crosses over to VRH in the bulk in agreement with observations in the present samples. However, power laws in bias that are characteristic of mesoscopic samples seem to survive even in bulk samples. A clue to such behavior may possibly lie in the heterogeneous structure of a CP which may be viewed to consist of multitudes of thin filmlike structure embedded inside the bulk.[12,13] The conductance corresponding to two-step tunneling is proportional to $\exp(-w/3a)$. Obviously, w cannot be a macroscopic sample size (10^{-6} to 0.1 cm); rather, it must be of the order of width of the disordered region along a polymer fibril, which may be order of 5 nm.[13] Then it is not clear why power laws in temperature do not survive in the bulk. Furthermore, since Ohmic–non-Ohmic transition is a continuous process, the transformation of a percolative[58] trajectory of a charge carrier in VRH (Ohmic) regime (top panel of Fig. 14) to a linear trajectory in the non-Ohmic regime (bottom panel of Fig. 14) must be pretty abrupt. Apparently, such an abrupt behavior has been reported when $w \sim R_h$ in three dimensions, although a precise theory is lacking.[49] Finally, it is a sort of role reversal for temperature at two limits of sample dimension.

When the latter is of the order of a few hopping lengths, the optimal number of localized states[50] is roughly given by $n_{\rm opt} = w/R_h - 1$, where R_h is given by Eq. (8). Since R_h increases with decreasing temperature, $n_{\rm opt}$ decreases. However, as seen in Fig. 6, *I-V* curves become increasingly non-Ohmic, and hence $n_{\rm opt}$ increases, with decreasing temperature. To summarize, the scaling function Eq. (15) derived from the GM expression Eq. (12) under certain assumptions provides an excellent description of the experimental data, satisfies general requirements of scaling Eqs. (4) and (6), and yields an expression Eq. (20) for the nonlinearity exponent. However, theoretical efforts are necessary to validate the assumptions and to remove contradictions.

Apart from the conceptual problems outlined above, we list here the interesting features involving particularly the coefficients σ_n that were observed and need to be explained theoretically. First is the incidence of channel selection in macroscopic samples. It is necessary to understand the exact conditions in the GM model that allow such a selection phenomenon and then how those conditions may be satisfied in CPs. Second is the assumption Eq. (14) that makes scaling analysis possible within the GM model. Third is Eq. (18), which relates each channel coefficient to the linear conductivity. Simple arguments yield only $y_n < 1$ for $n > 1$ Eq. (19). However, $y_n > 1$ is necessary to have negative nonlinearity exponents. Fourth is the physical process that limits the number of channels to a finite value in a given system.

VI. CONCLUSION

In this paper, we have reported field-dependent conductivities in various lightly doped CP systems as a function of temperature and quenched disorder. We demonstrated that each of the various CP systems possesses a *single* field scale and exhibits the associated scaling. A phenomenological scaling equation that led to the extraction of nonlinear exponents was used to analyze the nonlinear transport data. It was argued that experimental evidence points to the linear conductivity as a natural scaling variable. Surprisingly, the GM expression for multistep tunneling proves to be an excellent fit to the *I-V* curves as well as the scaled curves. A couple of assumptions are made to make the GM model compatible with scaling. Experimental values of the exponents fall within the predicted limits of $-1/2$ and $3/4$. A theory capable of explaining the nonlinear exponents, particularly negative ones, is lacking. The value of the exponent depends upon the path of measurement in the variable space. Some issues concerning applicability of the GM model to CPs have been discussed.

The scaling that has been observed in CPs has been also found in many other disordered systems including composites. It is believed that such scaling may be truly a universal feature of disordered systems, particularly with localized states. All the samples considered here are three dimensional. It will be interesting to know how such scaling fares in lower dimensions. It is hoped that the results presented here will lead to increased theoretical efforts to understand scaling phenomena in field-dependent transport in disordered systems.

ACKNOWLEDGMENTS

This work was supported in part by the Department of Science and Technology, Government of India, through Major Research Project No. SR/S2/CMP-0054/2008.

*kamalk.bardhan@saha.ac.in

[1] A. J. Epstein, in *Physical Properties of Polymers Handbook*, edited by J. E. Mark (Springer-Verlag, Berlin, 2006), pp. 15–17.
[2] Y. Z. Wang, D. D. Gebler, D. K. Fu, T. M. Swager, and A. J. Epstein, Appl. Phys. Lett. **70**, 3215 (1997).
[3] Gary P. Kushto, Woohong Kim, and Zakya H. Kafafi, Appl. Phys. Lett. **86**, 093502 (2005).
[4] M. S. Lee, H. S. Kang, H. S. Kang, J. Joo, A. J. Epstein, and J. Y. Lee, Thin Solid Films **477**, 169 (2005).
[5] J. Joo, J. K. Lee, S. Y. Lee, K. S. Jang, E. J. Oh, and A. J. Epstein, Macromolecules **33**, 5131 (2000).
[6] C. C. Bof Bufon, J. Vollmer, T. Heinzel, P. Espindola, H. John, and Jürgen Heinze, J. Phys. Chem. B **109**, 19191 (2005).
[7] A. J. Heeger, S. Kivelson, J. R. Schrieffer, and W.-P. Su, Rev. Mod. Phys. **60**, 781 (1988).
[8] T. Ishiguro, H. Kaneko, Y. Nogami, H. Ishimoto, H. Nishiyama, J. Tsukamoto, A. Takahashi, M. Yamaura, T. Hagiwara, and K. Sato, Phys. Rev. Lett. **69**, 660 (1992).
[9] K. Lee, S. Cho, S. H. Park, A. J. Heeger, C.-W. Lee, and S.-H. Lee, Nature (London) **441**, 65 (2006).
[10] A. B. Kaiser, Adv. Mater. **13**, 927 (2001).
[11] A. B. Kaiser, Rep. Prog. Phys. **64**, 1 (2001).
[12] J. Joo, Z. Oblakowski, G. Du, J. P. Pouget, E. J. Oh, J. M. Wiesinger, Y. Min, A. G. MacDiarmid, and A. J. Epstein, Phys. Rev. B **49**, 2977 (1994).
[13] V. N. Prigodin and A. J. Epstein, Synth. Met. **125**, 43 (2002).
[14] W. R. Salaneck, I. Lundstrom, and B. Ranby, in *Conjugated Polymers and Related Materials*, edited by Y. E. Whang and S. Miyata (Oxford Science, Oxford, 1993), Chap. 11, p. 149.
[15] V. C. Nguyen and K. Potje-Kamloth, Thin Solid Films **338**, 142 (1999).
[16] G. B. Street, in *Handbook of Conducting Polymer*, edited by T. A. Skotheim (Dekker, New York, 1986), p. 265.
[17] J. Kim, E. Kim, Y. Won, H. Lee, and K. Suh, Synth. Met. **139**, 485 (2003).
[18] Q. Pei, G. Zuccarello, M. Ahlskog, and O. Inganäs, Polymer **35**, 1347 (1994).
[19] Liam S. C. Pingree, Bradley A. MacLeod, and David S. Ginger, J. Phys. Chem. C **112**, 7922 (2008).
[20] C. O. Yoon, M. Reghu, D. Moses, and A. J. Heeger, Phys. Rev. B **49**, 10851 (1994).
[21] A. Bhattacharya, A. De, S. N. Bhattacharya, and S. Das, J. Phys. Condensed Matter. **6**, 10499 (1994).
[22] S. Maji, S. Mukhopadhyay, R. Gangopadhyay, and A. De, Phys. Rev. B **75**, 073202 (2007).
[23] J. M. Ribo, M. C. Anglada, J. M. Hernandez, X. Zhang, N. F. Anglada, A. Chaibi, and B. Movaghar, Synth. Met. **97**, 229 (1998).
[24] A. N. Aleshin, J. Y. Lee, S. W. Chu, S. W. Lee, B. Kim, S. J. Ahn, and Y. W. Park, Phys. Rev. B **69**, 214203 (2004).

[25]C. C. Bof Bufon and T. Heinzel, Phys. Rev. B **76**, 245206 (2007).
[26]N. F. Mott, Philos. Mag. **19**, 835 (1969).
[27]A. L. Efros and B. I. Shklovskii, J. Phys. C **8**, 49 (1975).
[28]J. G. Park, S. H. Lee, H. Y. Yu B. Kim, J. H. Park, M. S. Kabir, S. Kubatmin, M. Persson, A. B. Kaiser, and Y. W. Park, Curr. Appl. Phys. **2**, 23 (2002).
[29]J. G. Park, B. Kim, S. H. Lee, A. B. Kaiser, S. Roth, and Y. W. Park, Synth. Met. **135**, 229 (2003).
[30]J. G. Park, B. Kim, S. H. Lee, and Y. W. Park, Thin Solid Films **438**, 118 (2003).
[31]A. B. Kaiser, S. A. Rogers, and Y. W. Park, Mol. Cryst. Liq. Cryst. **415**, 115 (2004).
[32]A. B. Kaiser and Y. W. Park, Synth. Met. **152**, 181 (2005).
[33]Zhi-Hua Yin, Yun-Ze Long, Chang-Zhi Gu, Mei-Xiang Wan, and Jean-Luc Duvail, Nanoscale Res. Lett. **4**, 63 (2009).
[34]R. M. Hill, Philos. Mag. **24**, 1307 (1971).
[35]B. I. Shklovskii, Fiz. Tekh. Poluprov. **6**, 2335 (1973) [Sov. Phys. Semicond. **6**, 1964 (1973)].
[36]M. Pollak and I. Riess, J. Phys. C **9**, 2339 (1976).
[37]B. I. Shklovskii, Fiz. Tekh. Poluprov. **10**, 1440 (1976) [Sov. Phys. Semicond. **10**, 855 (1976)].
[38]P. Sheng, E. K. Sichel, and J. I. Gittleman, Phys. Rev. Lett. **40**, 1197 (1978).
[39]L. I. Glazman and K. A. Matveev, Zh. Eksp. Teor. Fiz. **94**, 332 (1988) [Sov. Phys. JETP **67**, 1276 (1988)].
[40]D. Talukdar, K. K. Bardhan, and U. N. Nandi (unpublished).
[41]K. K. Bardhan, Physica A **241**, 267 (1997).
[42]E. Abrahams, P. W. Anderson, D. C. Licciardello, and T. V. Ramakrishnan, Phys. Rev. Lett. **42**, 673 (1979).
[43]H. E. Stanley, *Introduction to Phase Transitions and Critical Phenomena* (Oxford University Press, New York, 1971).
[44]Y. Gefen, W. H. Shih, R. B. Laibowitz, and J. M. Viggiano, Phys. Rev. Lett. **57**, 3097 (1986).
[45]R. K. Chakrabarty, K. K. Bardhan, and A. Basu, Phys. Rev. B **44**, 6773 (1991).
[46]F. Ladieu, D. L'Hote, and R. Tourbot, Phys. Rev. B **61**, 8108 (2000), and references therein.
[47]M. Morgan and P. A. Walley, Philos. Mag. **23**, 661 (1971). A. Servini and A. K. Jonscher, Thin Solid Films **3**, 341 (1969).
[48]D. Yu, C. Wang, B. L. Wehrenberg, and P. Guyot-Sionnest, Phys. Rev. Lett. **92**, 216802 (2004).
[49]Y. Xu, D. Ephron, and M. R. Beasley, Phys. Rev. B **52**, 2843 (1995).
[50]A. I. Yakimov, N. P. Stepina, and A. V. Dvurechenskii, J. Phys. Condens. Matter **6**, 2583 (1994).
[51]C. Hófener, J. B. Philipp, J. Klein, L. Alff, A. Marx, B. Búchner, and R. Gross, Europhys. Lett. **50**, 681 (2000).
[52]V. Markovich, G. Jung, I. Fita, D. Mogilyansky, X. Wu, A. Wisniewski, R. Puzaniak, L. Titelman, L. Vradman, M. Herskowitz, and G. Gorodetsky, J. Magn. Magn. Mater. **322**, 1311 (2010).
[53]The exponent is 1.75 according to Ref. 24.
[54]U. N. Nandi, K. K. Bardhan, and C. D. Mukherjee, Mater. Sci. Forum **223**, 261 (1996).
[55]D. Stauffer and A. Aharony, *Introduction to Percolation Theory*, 2nd ed. (Taylor and Francis, London, 1992).
[56]A. V. Tartakovskii, M. V. Fistul, M. E. Raikh, and I. M. Ruzin, Sov. Phys. Semicond. **21**, 370 (1987).
[57]E. I. Levin, I. M. Ruzin, and B. I. Shklovskii, Fiz. Tekh. Polup. **22**, 624 (1988) [Sov. Phys. Semicond. **22**, 401 (1988)].
[58]B. I. Shklovskii and A. L. Efros, *Electron Properties of Doped Semiconductors* (Springer Verlag, Berlin, 1984).